

# Linear optical response from the *odd* parity Bardasis-Schrieffer mode in locally non-centrosymmetric superconductors

Changhee Lee<sup>1</sup> and Suk Bum Chung<sup>2,3,\*</sup>

<sup>1</sup>*Department of Physics and Astronomy, Seoul National University, Seoul 08826, Korea*

<sup>2</sup>*Department of Physics and Natural Science Research Institute, University of Seoul, Seoul 02504, Korea*

<sup>3</sup>*School of Physics, Korea Institute for Advanced Study, Seoul 02455, Republic of Korea*

(Dated: December 29, 2022)

On the recent report of a magnetic field induced first order transition between an even-parity superconductivity and an odd-parity superconductivity in CeRh<sub>2</sub>As<sub>2</sub> [Khim *et al.* *Science*, **373**, 1012 (2021)], the microscopic physics is still under investigation. However, if, in the vicinity of this transition, the coupling strengths of the even and odd pairing channels are comparable, a particle-particle excitonic collective mode referred to as the Bardasis-Schrieffer (BS) mode should generically exist below the pair-breaking continuum. This BS mode can couple to the light and thus affect the optical response of the superconductor, as it arises from a pairing channel with the parity opposite to that of the ground state pairs. Here, by using a generic bilayer model Hamiltonian for the electronic degree of freedom, which is globally centrosymmetric despite each layer being locally non-centrosymmetric, we study the change of the excitation gap of the BS mode with respect to the out-of-plane magnetic fields and demonstrate that its coupling to the light is possible even in the linear response regime. The linear coupling is attributed to the presence of multiple electronic bands, which is a generic feature of a bilayer system. Our result shows the microwave absorption as the signature of the BS mode, and hence a smoking gun signature of the parity-switching at the transition between two superconducting phases.

## I. INTRODUCTION

Discovering superconductors with odd-parity Cooper pairing has been a long-standing challenge in condensed matter physics, as they are rare in inversion symmetric solid state systems. To name a few, UPt<sub>3</sub> [1], UNi<sub>2</sub>Al<sub>3</sub> [2] and Sr<sub>2</sub>RuO<sub>4</sub> [3] are the most notable candidates which have been suspected to host odd-parity Cooper pairings for a long time, though the case of a much studied candidate material Sr<sub>2</sub>RuO<sub>4</sub> has grown more controversial in recent years [4–8].

Faced with this rarity of odd-parity superconducting materials, many research have endeavored to find realistic conditions favoring the odd parity superconductivity. For instance, the systems possessing a structural instability toward an inversion-symmetry-broken phase such as the pyrochlore oxide Cd<sub>2</sub>Re<sub>2</sub>O<sub>7</sub> drew attention for a potential to host an odd-parity superconducting phase [9–12].

Another mechanism for odd-parity superconductivity is suggested by a recent experiment on CeRh<sub>2</sub>As<sub>2</sub> [13, 14]. There a transition is observed when the external magnetic fields are applied along the *c*-axis within the superconducting phase of CeRh<sub>2</sub>As<sub>2</sub> [13]. According to the preceding theoretical studies [15, 16], the transition referred to as the even-to-odd transition seems to occur between two superconducting phases of opposite parities under an inversion. The Pauli paramagnetic pair-breaking effect [17, 18] is a known mechanism for destroying the even-parity superconducting

(eSC) phase. By contrast, an odd-parity superconducting (oSC) state can withstand the magnetic fields through an equal-(pseudo)spin pairing [13, 19–21]. It is noted that the combination of *P4/nmm* nonsymmorphic crystal structure and the heavy-fermion characteristic supports strong intralayer Rashba-type spin-orbit couplings that are known to favor equal-(pseudo)spin pairings [20].

An intriguing implication of the even-to-odd transition in CeRh<sub>2</sub>As<sub>2</sub> is that the coupling strengths of the attractive interactions for both pairing channels may be comparable. The potential transition temperature  $T_{c,o}$  of the oSC phase at the zero-field, which is preempted by the onset of the eSC phase in reality, is estimated to be close to the transition temperature  $T_{c,e}$  of the eSC phase [13]. Moreover, phenomenological studies have reproduced the overall superconducting phase diagram in CeRh<sub>2</sub>As<sub>2</sub> with comparable coupling strengths for both pairing channels [13, 22].

Even if the most of the theories set forth so far support that the high-field superconducting phase of CeRh<sub>2</sub>As<sub>2</sub> is odd in parity, counter-arguments have also been raised. For instance, a theoretical study proposed that the observed magnetic field induced phase transition arises not from the parity switching of the superconducting gap but from the spin-flopping in the coexistent antiferromagnetic order parameter [23]. Therefore, further experimental signatures need to be sought for the first-order transition that switches the parity of the superconducting gap. Of the many ways to find an indisputable evidence for the symmetry of the superconducting phase, one is to investigate the collective modes in the superconducting phase. Historically, the detection of a number of the nearly-degenerate collective modes in the superfluid *B*-

\* sbchung0@uos.ac.kr

phase of  $^3\text{He}$  proved to be the decisive evidence in favor of the spin-triplet pairing [24].

In this regards, we note that, if the even-to-odd transition is really a parity-switching transition,  $T_{c,o} \approx T_{c,e}$ , which implies the close competition between two pairing channels of opposite parities, provides a favorable condition for a collective mode, known as the Bardasis-Schrieffer (BS) mode [25], to appear far from the pair-breaking continuum. The BS mode is an exciton-like collective mode in superconductors due to a sub-leading pairing channel and indicates an instability towards another superconducting phase breaking some symmetries of the superconducting ground state. As a precursor of the instability of the superconducting ground state, the gap of the BS mode becomes smaller as the sub-leading channel gets stronger. However, such closely competing pairing channels have been rarely been found in superconductors, with one of a few exceptions being the iron-based superconductors, where the close competition between the  $s$ -wave and  $d$ -wave pairing channels have been confirmed by the Raman detection of the BS mode [26, 27].

Besides the possible existence of the BS mode, it is worth noting that the collective mode can possess a non-zero optical coupling when the parity of the sub-leading pairing channel under inversion is the opposite of that of the superconducting ground state. This feature makes the detection of the collective mode possible through the optical response in the *linear* response regime, which can be thought of as a compelling proof for the existence of a strong odd-parity pairing channel. This is in a sharp contrast to the Fe-based superconductors where the electronic Raman spectroscopy is used to detect the BS mode from the  $d$ -wave channel as this pairing channel and the  $s$ -wave ground state pairing share the same parity [26, 27]. Thus, in the case of  $\text{CeRh}_2\text{As}_2$ , the detection of the BS mode would be a smoking gun evidence for the occurrence of the parity-switching at the observed transition between the two superconducting phases.

In this work, we conduct a qualitative study on the BS modes in the clean limit superconducting phase of a locally non-centrosymmetric system such as  $\text{CeRh}_2\text{As}_2$ , which arise from the odd-parity and even-parity pairing channel in the eSC state and oSC state, respectively. First, we demonstrate the even-to-odd parity transition by the Pauli paramagnetic effect at the zero-temperature at the level of a mean-field description. We then briefly introduce the generalized random phase approximation (GRPA) [28, 29] which provides the basis of the analysis in this work. Also, it is shown that the BS modes from the subdominant pairing channels can be linearly coupled to the light. This is ascribed to the origin of the BS mode whose parity is opposite to the ground state Cooper pairing. Using the GRPA, we investigate the softening of the BS modes under the external magnetic fields along  $c$ -axis and the linear optical response from the BS modes.

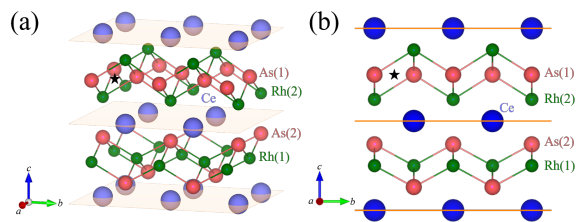


Figure 1. Crystal structure of  $\text{CeRh}_2\text{As}_2$ . (a) Bird's eye view of the structure. (b) A view from the (100) direction. An inversion center is marked by a black star.

## II. FIRST ORDER TRANSITION BY PAULI PARAMAGNETIC PAIR-BREAKING

To discuss the BS mode under the external magnetic field, the critical magnetic fields for the even-to-odd transition in the superconducting phase should be found first. Thus, we start our presentation by demonstrating the even-to-odd transition in the superconducting phase in a locally non-centrosymmetric layered structure by using a mean-field description at the zero-temperature. For results valid in a more wide range of temperature and magnetic fields, we refer to Refs. [15, 16, 21, 30].

Let us begin with a model Hamiltonian for the normal phase of the representative locally non-centrosymmetric system,  $\text{CeRh}_2\text{As}_2$ , subject to the point group  $D_{4h}$  which is given by [13, 16, 20, 21]:

$$H_0(\mathbf{k}) = \sum_{i=0}^2 \varepsilon_{i0}(\mathbf{k})\sigma_i + \sum_{i=1}^3 \varepsilon_{3i}(\mathbf{k})\sigma_3 s_i - \mu \quad (1)$$

with

$$\varepsilon_{00}(\mathbf{k}) = 2t(2 - \cos k_x - \cos k_y), \quad (2)$$

$$\varepsilon_{10}(\mathbf{k}) = t_{c,1} \cos \frac{k_z}{2} \cos \frac{k_x}{2} \cos \frac{k_y}{2}, \quad (3)$$

$$\varepsilon_{20}(\mathbf{k}) = t_{c,2} \sin \frac{k_z}{2} \cos \frac{k_x}{2} \cos \frac{k_y}{2}, \quad (4)$$

$$\varepsilon_{31}(\mathbf{k}) = -\alpha_R \sin k_y, \quad (5)$$

$$\varepsilon_{32}(\mathbf{k}) = \alpha_R \sin k_x, \quad (6)$$

$$\varepsilon_{33}(\mathbf{k}) = \lambda_I \sin k_z \sin k_x \sin k_y (\cos k_x - \cos k_y), \quad (7)$$

where  $\sigma_i$  and  $s_i$  are the Pauli matrices for the orbital and spin degrees of freedom, respectively. Here, two orbital degrees of freedom are introduced to take account of the locally non-centrosymmetric feature of the system. The reason is easily understood by looking into the crystal structure of  $\text{CeRh}_2\text{As}_2$  drawn in Figure 1. In Fig. 1(a), the crystal structure is depicted with three  $\{001\}$  lattice planes composed of Ce atoms. The locally broken inversion symmetry around Ce atoms is easily noted in Fig. 1(b) where the crystal structure is viewed from the (100) direction. The black stars in Fig. 1 correspond to a center for the global inversion symmetry, under which no individual atom is left invariant. This global inversion

is represented by  $\mathcal{P} = \sigma_1 s_0$  in the basis of the model Hamiltonian  $H_0(\mathbf{k})$  in Eq. (1).

$t_{c,1}$  and  $t_{c,2}$  are the hoppings between the nearest-neighbor Ce layers depicted in Fig. 1. These hoppings endow the three-dimensional characteristics to the electronic structure.  $\alpha_R$  and  $\lambda_I$  denote the intra-layer Rashba- and inter-layer Ising-type spin-orbit couplings, respectively. Note that the sign of the Rashba spin-orbit coupling alternate layer by layer, which reflects the locally non-centrosymmetric structure of the system shown in Fig. 1(b).

Throughout this work, we ignore  $\lambda_I$  since this spin-orbit coupling corresponds to a spin-dependent inter-layer hopping between the two *next*-nearest-neighbor layers, and thus it is expected to be much weaker than the spin-independent inter-layer hoppings  $t_{c,1}$ ,  $t_{c,2}$  between the nearest layers and the intra-layer Rashba spin-orbit coupling  $\alpha_R$ . Also, we assume that the Rashba-type spin-orbit coupling  $\alpha_R$  is much larger than the intra-layer hoppings  $t_{c,1}$  and  $t_{c,2}$  following Refs. [13, 20]. In this limit of large Rashba spin-orbit coupling, the difference between  $t_{c,1}$  and  $t_{c,2}$  has no significant effect on the band structure except for a weak modulation of the Fermi surface along the  $k_z$ -axis. Thus,  $t_c \equiv t_{c,1} = t_{c,2}$  is assumed throughout this work.

The two-fold degenerate eigenenergies of  $H_0(\mathbf{k})$  in Eq. (1) are given by

$$\xi_1(\mathbf{k}) = \varepsilon_{00}(\mathbf{k}) - \mu + \sqrt{t(\mathbf{k})^2 + \alpha(\mathbf{k})^2}, \quad (8)$$

$$\xi_2(\mathbf{k}) = \varepsilon_{00}(\mathbf{k}) - \mu - \sqrt{t(\mathbf{k})^2 + \alpha(\mathbf{k})^2}, \quad (9)$$

with  $t(\mathbf{k}) = \sqrt{\varepsilon_{10}(\mathbf{k})^2 + \varepsilon_{20}(\mathbf{k})^2}$  and  $\alpha(\mathbf{k}) = \sqrt{\varepsilon_{31}(\mathbf{k})^2 + \varepsilon_{32}(\mathbf{k})^2}$ . The eigenvectors of these eigenvalues are

$$|\xi_1, \alpha\rangle = \begin{pmatrix} \frac{\cos \frac{\chi}{2}}{\sqrt{2}} \\ e^{i\phi} \sin \frac{\chi}{2} \\ e^{i\zeta} \cos \frac{\chi}{2} \\ \frac{\sqrt{2}}{z \sin \frac{\chi}{2}} \\ -\sqrt{2} \end{pmatrix}, \quad |\xi_1, \beta\rangle = \begin{pmatrix} \frac{\sin \frac{\chi}{2}}{z\sqrt{2}} \\ e^{-i\zeta} \cos \frac{\chi}{2} \\ e^{-i\phi} \sin \frac{\chi}{2} \\ -\sqrt{2} \\ \frac{\cos \frac{\chi}{2}}{\sqrt{2}} \end{pmatrix}, \quad (10a)$$

$$|\xi_2, \alpha\rangle = \begin{pmatrix} \frac{\cos \frac{\chi}{2}}{z\sqrt{2}} \\ e^{-i\zeta} \sin \frac{\chi}{2} \\ -\sqrt{2} \\ e^{-i\phi} \cos \frac{\chi}{2} \\ -\sqrt{2} \\ \frac{\sin \frac{\chi}{2}}{-\sqrt{2}} \end{pmatrix}, \quad |\xi_2, \beta\rangle = \begin{pmatrix} \frac{\sin \frac{\chi}{2}}{\sqrt{2}} \\ e^{i\phi} \cos \frac{\chi}{2} \\ -\sqrt{2} \\ e^{i\zeta} \sin \frac{\chi}{2} \\ \frac{\sqrt{2}}{z \cos \frac{\chi}{2}} \end{pmatrix}, \quad (10b)$$

with  $\exp(i\chi) = \{t(\mathbf{k}) + i\alpha(\mathbf{k})\}/\sqrt{t(\mathbf{k})^2 + \alpha(\mathbf{k})^2}$ ,  $\exp(i\zeta) = \{\varepsilon_{10}(\mathbf{k}) + i\varepsilon_{20}(\mathbf{k})\}/t(\mathbf{k})$ ,  $\exp(i\phi) = \{\varepsilon_{31}(\mathbf{k}) + i\varepsilon_{32}(\mathbf{k})\}/\alpha(\mathbf{k})$ , and  $z = \exp[i(\zeta + \phi)]$ .

Provided this lattice model, we assume that two pairing channels whose form factors are represented by  $\sigma_0$  and  $\sigma_z$  are the predominant pairing channels in eSC and oSC states, respectively, which are used to reproduce the  $H - T$  phase diagram of  $\text{CeRh}_2\text{As}_2$  in Refs. [13, 20, 21, 30]. The gap function  $\sigma_0$  in the eSC state is uniform while the sign of the gap function  $\sigma_z$  alternates

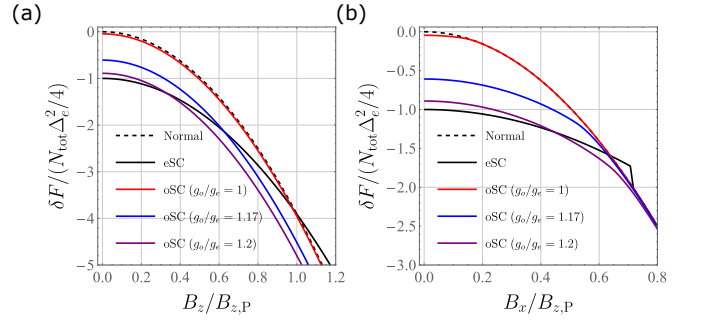


Figure 2. Free energy comparison of the normal phase and the superconducting phases. (a) Under the out-of-plane magnetic fields. (b) Under the in-plane magnetic fields. For comparison, the horizontal axes of both figures are normalized by the same  $B_{z,P}$ . The dashed line and the solid black line represent the free energies of the normal phase and the eSC phase, respectively. They meet at  $B_z = B_{z,P}$ . The red, blue, purple lines are the free energies of oSC states for  $g_o/g_e = 1, 1.17, 1.2$ . When these lines (oSC) cross the black solid line (eSC), the even-to-odd transition occurs. The parameters  $t = 2$ ,  $\mu = 0.5$ ,  $t_{c,1} = t_{c,2} = 0.1$ ,  $\alpha_R = 0.34$  and  $\Delta_e = 0.004$  are used. The ratio of  $\alpha$  and  $t_{c,1} = t_{c,2}$  is adopted from Refs. [13, 20].

layer-by-layer in the oSC state. Including the Zeeman term  $\mathbf{B} \cdot \mathbf{s}$ , the Bogoliubov-de Gennes (BdG) Hamiltonians for the eSC and oSC states are given by

$$H_{\text{BdG}}^{(p)}(B, \mathbf{k}) = \tau_0 \mathbf{B} \cdot \mathbf{s} + \tau_z H_0(\mathbf{k}) + \Delta_p \tau_x^{(p)}, \quad (11)$$

with  $p = e, o$  and  $\tau_i^{(p)} = \tau_i M_p$  for  $i = x, y, z$  where  $M_e = \sigma_0$  and  $M_o = \sigma_z$  are the pairing form factors, respectively. The magnetic field along (perpendicular) the  $z$ -axis, which corresponds to the  $c$ -axis of  $\text{CeRh}_2\text{As}_2$ , is denoted by  $B_z$  ( $B_x$ ) and it is referred to as the out-of-plane (in-plane) magnetic field in this work. Here, the basis field operator of the BdG Hamiltonian is  $\hat{\Psi}_{\mathbf{k}} = (\hat{C}_{\mathbf{k}}, \hat{C}_{-\mathbf{k}}^{\dagger T}(i s_y))^T$  [31, 32]. The gap amplitude  $\Delta_p$  presumed to be real is determined from the gap equation:

$$\Delta_p = \frac{g_p}{2} \sum_{\mathbf{k}} \text{Tr}[\tau_x^{(p)} G_{\mathbf{k}}^{(p)}], \quad (12)$$

with  $G_{\mathbf{k}}^{(p)} = i\omega - H_{\text{BdG}}^{(p)}(\mathbf{k})$ . Here,  $\sum_{\mathbf{k}} = (\beta V)^{-1} \sum_{\mathbf{k}}$  is the normalized summation over  $\mathbf{k} = (i\omega, \mathbf{k})$  a pair of Matsubara frequency and the three-dimensional momentum, where  $\beta = 1/k_B T$  and  $V$  are the inverse of the temperature and the volume of the system, respectively. The coupling constants  $g_e$  and  $g_p$  are assumed to be constant for the simplicity of the presentation. This assumption is valid in the weak-coupling regime which we are interested in for the qualitative study. Also, we refer to the superconducting phase with  $\Delta_p$  as  $p$ SC with  $p = e$  or  $o$  from now on.

The even-to-odd phase transition is determined by comparing the zero temperature (Gibbs) free energies of

eSC and oSC phases which are calculated through

$$\mathcal{F}_p(B_z) = \frac{\Delta_p^2}{4g_p} + \sum_{\mathbf{k}} \frac{\text{Tr}[H_0(\mathbf{k})] - \sum_n E_n^{(p)}(B_z, \mathbf{k})}{2} \quad (13)$$

with the positive energy  $E_n^{(p)}(B_z, \mathbf{k})$  of the BdG Hamiltonian  $H_{\text{BdG}}^{(p)}(B_z, \mathbf{k})$ . Fig. 2(a) illustrates the free energies of the normal, eSC, and oSC phases from which the normal phase free energy in the zero-field is subtracted. The parameters used are written in the caption of Fig. 2. The qualitative features of the system are well displayed with this set of parameters.  $g_e$  is chosen so that  $\Delta_e = 0.004$  is obtained by Eq. (12), which is used throughout this work unless otherwise noted.

Each curve in Fig. 2(a) is well described by

$$\mathcal{F}_p(B_z) = \mathcal{F}_p(0) - \frac{1}{2} \chi_{\text{spin}}^{(p)} B_z^2, \quad (14)$$

where the curvatures  $\chi_{\text{spin}}^{(p)}$  of the curves are understood as the spin susceptibility of the  $p$ SC state, while  $\chi_{\text{spin}}^{(n)}$  denotes the normal phase spin susceptibility. The cross point at the Pauli-limiting field  $B_z = B_{z,P}$  between the normal (black dashed line) and eSC (black line) phases marks the first order transition between the normal and eSC phase. Using Eq. (14),  $B_{z,P}$  is given by

$$B_{z,P} = \sqrt{\frac{\mathcal{F}_n(0) - \mathcal{F}_e(0)}{(\chi_{\text{spin}}^{(n)} - \chi_{\text{spin}}^{(e)})/2}}. \quad (15)$$

Compared to the conventional Pauli-limiting critical field referred to as the Chandrasekhar-Clogston field  $B_{z,CC} = \sqrt{2\{\mathcal{F}_n(0) - \mathcal{F}_e(0)\}/\chi_{\text{spin}}^{(n)}}$ ,  $B_{z,P}$  is several times larger because of the non-vanishing  $\chi_{\text{spin}}^{(e)}$  due to the sizable Rashba spin-orbit couplings [15, 33].

The red, blue, and green lines denote the oSC free energies with  $g_o = g_e$ ,  $g_o = 1.17g_e$  and  $g_o = 1.2g_e$ . Since  $\chi_{\text{spin}}^{(o)} = \chi_{\text{spin}}^{(n)}$  as shown in Fig. 2(a), the transition due to the Pauli paramagnetic depairing does not occur between the normal phase and the oSC state. The crossing point between the free energies of eSC and oSC phases for a given  $g_o$  indicates the even-to-odd transition observed in the experiment [13]. Moreover, the slope of the free energies at the crossing point are different which means the transition is of the first order and the magnetization changes discontinuously at the transition.

Note that eSC state can be more stable than the oSC state at the zero-field even if  $g_o > g_e$ , because the inter-layer spin-independent hoppings  $\varepsilon_{10}$  and  $\varepsilon_{20}$  effectively weakens  $g_o$ . The critical ratio  $r_c \equiv g_{o,c}/g_e$ , for which we obtain 1.207 for the aforementioned parameters, depends on the model parameters  $t$ ,  $\mu$ ,  $\alpha_R$ , *etc.* Above the critical ratio, the oSC state is the superconducting ground state of the system at the zero-field. In the two-dimensional limit in which the ratio  $\alpha_R/\max(|t_{c,1}|, |t_{c,2}|)$  is infinite, the electrons do not discern the trivial gap function  $\sigma_0$

from the sign-alternating gap function  $\sigma_z$ , and thus  $r_c \rightarrow 1$ .

Though the out-of-plane magnetic field is of our main interest, we present the free energies under the in-plane magnetic field as well. Fig. 2(b) displays the free energies of the normal and superconducting phases with in-plane magnetic fields  $\mathbf{B} = B_x \hat{\mathbf{x}}$ . The free energies of the normal and the eSC phase cross at the Pauli-limiting in-plane magnetic field  $B_{x,P}$  which is smaller than  $B_{z,P}$ , and this is consistent with the experiment [13, 34]. When it comes to the oSC state, we do not see a first order transition to the normal phase due to the Pauli depairing, while an exponential decrease of the gap function is seen with the increasing in-plane magnetic fields [See Appendix B for details].

Furthermore, it seems practically impossible to observe the first order even-to-odd transition induced by the in-plane magnetic fields even when  $g_o/g_e$  is larger than 1 unless sufficiently close to the critical value. For example, when  $g_o/g_e = 1.2$ , there is a fair range of  $B_x$  in which the oSC state is more stable than the eSC state. However, for an intermediate ratio like  $g_o/g_e = 1.17$ , the distance between the free energies of the oSC phase and the normal phase is very narrow when the free energies of the eSC and the oSC states are comparable. Up to the impurity and finite-temperature effects,  $g_o/g_e \geq 1$  is consistent with the experimental result where a phase transition by the in-plane magnetic field is not identified [13].

Thus far, we have demonstrated that the BdG model Hamiltonian with the Zeeman term for the locally non-centrosymmetric system exhibits a first order even-to-odd phase transition in the superconducting phase under the out-of-plane magnetic fields at the zero-temperature. An interesting point, not captured by the mean-field analysis, is that first order transitions usually accompany hysteresis because a system can still be in a metastable state. The range of the meta-stability can be related with a collective mode [35], especially the BS mode when a transition between two superconducting phases is concerned, which is the main subject of this work.

### III. BARDASIS-SCHRIEFFER MODE AROUND THE TRANSITION

#### A. Generalized Random Phase Approximation

To study the BS mode, we use the generalized random phase approximation (GRPA) [25, 28, 29, 36], which is one of the primary methods to incorporate the effect of the collective modes in the superconducting phase. Before applying the method to our case, we first briefly introduce the formulation of the generalized random-phase approximation.

Concerned with the linear optical response of the fluctuation from the subdominant pairing channels in a superconductor, we consider an attractive electronic inter-

action consistent with the gap equation in Eq. (12):

$$\hat{V} = -\frac{1}{2} \sum_p \sum_{k_1, k_2, q} g_p \hat{\Pi}_p(k_1, k_1 - q) [\hat{\Pi}_p(k_2, k_2 - q)]^\dagger, \quad (16)$$

where  $\hat{\Pi}_p(k_1, k_2) = \hat{\Psi}_{k_1}^\dagger \tau_\pm^{(p)} \hat{\Psi}_{k_2}$  with  $\tau_\pm^{(p)} = (\tau_x^{(p)} \pm i\tau_y^{(p)})/2$ .  $\sum_p$  is the summation over the pairing channels labeled by  $p = e$  and  $p = o$ . While the pairing interaction  $\hat{V}$  derived solely from the on-site attractive interaction would have given us  $g_o = g_e$ , a general pairing interaction gives us  $g_o \neq g_e$ . Thus we consider the cases with  $g_o \neq g_e$  as well as  $g_o = g_e$ . Other pairing channels such as those discussed in Refs. [21, 33] do not couple linearly to the light because of the symmetries of  $H_0$  with negligible  $\lambda_I$  [See Appendix A for details].

Adding  $\hat{V}$  to the normal phase action  $\mathcal{S}_0 = \frac{1}{2} \sum_k \hat{\Psi}_k^\dagger (i\omega - H_0) \hat{\Psi}_k$  and using the Hubbard-Stratonovich transformation, we obtain the following total action for pSC phase with pairing fluctuations under the external scalar and vector fields:

$$\mathcal{S} = \mathcal{S}_e^{(p)} + \mathcal{S}_{e-\eta} + \mathcal{S}_\eta + \mathcal{S}_{e-A}, \quad (17)$$

$$\mathcal{S}_e^{(p)} = \frac{1}{2} \sum_k \hat{\Psi}^\dagger(k) \{-i\omega + H_{\text{BdG}}^{(p)}(\mathbf{k})\} \hat{\Psi}(k), \quad (18)$$

$$\mathcal{S}_\eta = \frac{1}{2} \sum_{p,a} \sum_q \frac{\hat{\eta}_a^{(p)}(q) \hat{\eta}_a^{(p)}(-q)}{g_p}, \quad (19)$$

$$\mathcal{S}_{e-\eta} = \frac{1}{2} \sum_{p,a} \sum_{k,q} \hat{\Psi}^\dagger(k+q) \{\eta_a^{(p)}(q) \tau_a^{(p)}\} \hat{\Psi}(k), \quad (20)$$

$$\mathcal{S}_{e-A} = \frac{1}{2} \sum_{k,q} \hat{\Psi}^\dagger(k+q) \{\Gamma_1(\mathbf{k}, \mathbf{q}) + \Gamma_2(k, q)\} \hat{\Psi}(k). \quad (21)$$

The auxiliary bosonic fields  $\eta_1^{(p)}$  and  $\eta_2^{(p)}$  represent the real and imaginary parts of the fluctuation in the pairing channel  $M_p$ , respectively. They correspond to the amplitude and the phase fluctuation, respectively, when  $\Delta_p$  is real.  $\Gamma_1$  and  $\Gamma_2$  are the paramagnetic and diamagnetic light-matter coupling vertices, respectively, and expressed as

$$\Gamma_1(\mathbf{k}, q) = \sum_{\mu=0}^3 \mathcal{V}_\mu(\mathbf{k}, \mathbf{q}) \mathcal{A}_\mu(q), \quad (22)$$

$$\Gamma_2(k, q) = \sum_{k'} \sum_{i,j=1}^3 [m_{\mathbf{k}}^{-1}]_{ij} \mathcal{A}_i(q - k') \mathcal{A}_j(k'), \quad (23)$$

with the four-velocity operator  $\mathcal{V}_\mu(\mathbf{k}, \mathbf{q}) = (2\tau_z, \tau_0 \partial_i \{H_0(\mathbf{k} + \mathbf{q}) + H_0(\mathbf{k})\})/2$  and the inverse of the mass matrix  $[m_{\mathbf{k}}^{-1}]_{ij} = \tau_z \partial_i \partial_j H_0(\mathbf{k})$ . Here, we define a four-potential  $\mathcal{A}_\mu = |e|(-iA_0, \mathbf{A})$  by multiplying the unit charge  $|e|$  to the conventional four-potential for conciseness.

The effective action for  $\mathcal{A}_\mu$  and  $\eta_a^{(p)}$  is obtained by integrating out the fermionic degree of freedom  $\hat{\Psi}$  and

expanding the resultant action to the second order of  $\mathcal{A}_\mu$  and  $\eta_a^{(p)}$ :

$$\mathcal{S}_{\text{eff}} = \frac{1}{2} \sum_q (\mathcal{A}_\mu, \eta_a^{(p)})_{-q} \Lambda(q) \begin{pmatrix} \mathcal{A}_\nu \\ \eta_b^{(p')} \end{pmatrix}_q, \quad (24)$$

with

$$\Lambda(q) = \begin{pmatrix} K_{\mu\nu} & L_{\mu b}^{(p')} \\ R_{a\nu}^{(p)} & \frac{\delta_{pp'} \delta_{ab}}{g_p} + \Pi_{ab}^{(p,p')} \end{pmatrix}_q, \quad (25)$$

whose sub-blocks are given by

$$K_{\mu\nu}(q) = \frac{1}{2} \sum_k \text{Tr}[\mathcal{V}_\mu(\mathbf{k}, \mathbf{q}) G(k+q) \mathcal{V}_\nu(\mathbf{k}, \mathbf{q}) G(k)] + \sum_k \text{Tr}[G(k) [m_{\mathbf{k}}^{-1}]_{\mu\nu}], \quad (26)$$

$$L_{\mu a}^{(p)}(q) = \frac{1}{2} \sum_k \text{Tr}[\mathcal{V}_\mu(\mathbf{k}, \mathbf{q}) G(k+q) \tau_a^{(p)} G(k)], \quad (27)$$

$$R_{a\mu}^{(p)}(q) = \frac{1}{2} \sum_k \text{Tr}[\tau_a^{(p)} G(k+q) \mathcal{V}_\mu(\mathbf{k}, \mathbf{q}) G(k)], \quad (28)$$

$$\Pi_{ab}^{(p,p')}(q) = \frac{1}{2} \sum_k \text{Tr}[\tau_a^{(p)} G(k+q) \tau_b^{(p')} G(k)]. \quad (29)$$

Here,  $[m_{\mathbf{k}}^{-1}]_{\mu\nu}$  is zero when either of  $\mu$  or  $\nu$  is 0. The basic symmetry properties of the kernels are  $K_{\mu\nu}(q) = K_{\nu\mu}(-q)$ ,  $\Pi_{ab}^{(p,p')}(q) = \Pi_{ba}^{(p',p)}(-q)$ , and  $R_{a\mu}^{(p)}(q) = L_{\mu a}^{(p)}(-q) = [L_{\mu a}^{(p)}(q)]^*$ . The real-frequency kernels are obtained by the analytical continuation  $i\Omega \rightarrow \Omega^+ = \Omega + i\epsilon$ .  $\epsilon = 10^{-6} = 2.5 \times 10^{-4} \Delta_e$  is used throughout this work unless otherwise noted.

Note that  $H_{\text{BdG}}^{(e)}$  and  $H_{\text{BdG}}^{(o)}$  are invariant under the *inversion* symmetry operators  $\tau_0 \mathcal{I}$  and  $\tau_z \mathcal{I}$ , respectively. These symmetries of the BdG Hamiltonians provide a selection rule at  $\mathbf{q} = \mathbf{0}$ . Considering the parities of the vertices  $\mathcal{V}_\mu$  and  $\tau_a^{(M)}$  under the inversion symmetries of  $H_{\text{BdG}}^{(p)}$ , several components of the kernel  $\Lambda(i\Omega, \mathbf{0})$  are eliminated the kernel is reduced into two blocks:

$$\Lambda(i\Omega) \sim \begin{pmatrix} K_{00} & L_{0b}^{(p)} \\ R_{a0}^{(p)} & \tilde{\Pi}_{ab}^{(p)} \end{pmatrix} \oplus \begin{pmatrix} K_{ij} & L_{ib}^{(\bar{p})} \\ R_{aj}^{(\bar{p})} & \tilde{\Pi}_{ab}^{(\bar{p})} \end{pmatrix}, \quad (30)$$

where  $\tilde{\Pi}_{ab}^{(p)} = g_p^{-1} \delta_{ab} + \Pi_{ab}^{(p,p)}$ .  $\bar{p}$  denotes the odd-parity(even-parity) pairing channel in eSC(oSC) state, which is the subdominant pairing channel. Eqs. (24) and (30) explicitly show that the fluctuations of the dominant pairing channel are coupled to the density-density response  $K_{00}$  in the first block in Eq. (30) whereas the subdominant fluctuations are involved in the optical response in the second block in Eq. (24) when  $L_{ib}^{(\bar{p})}$  and  $R_{aj}^{(\bar{p})}$  are finite. To discuss the linear optical response of the fluctuation of the subdominant channel, we focus on the second block in the remainder of our presentation.

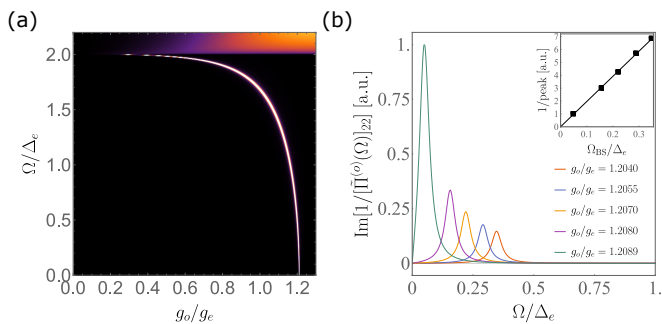


Figure 3. False color plot of  $\text{Im}[1/[\tilde{\Pi}^{(o)}(\Omega)]_{22}]$  on the  $g_o/g_e - \Omega$  plane in the eSC state. The energy  $\Omega$  of the incident light is normalized by the magnitude  $\Delta_e$  of the gap function in eSC state. (b)  $\text{Im}[1/[\tilde{\Pi}^{(o)}(\Omega)]_{22}]$  for several  $g_o/g_e$ . For (b),  $\epsilon = 10^{-4} = 2.5 \times 10^{-2} \Delta_e$  is exceptionally used. The inset plots the peak position in (b) and the inverse of the peak height in (b).

### B. Bardasis-Schrieffer mode at the zero-field

Armed with the GRPA method, we study the BS mode originating from the subdominant pairing fluctuation  $\eta_1^{(\bar{p})}$  and  $\eta_2^{(\bar{p})}$  [24, 25, 27, 36, 37]. The equation of motion for the BS mode is given by  $0 = \delta \mathcal{S}_{\text{eff}} / \delta \eta_{\alpha}^{(\bar{p})}$  which is rearranged into

$$\eta^{(\bar{p})}(\mathbf{q}) = -[\tilde{\Pi}^{(\bar{p})}(\mathbf{q})]^{-1} R^{(\bar{p})}(\mathbf{q}) \mathcal{A}(\mathbf{q}). \quad (31)$$

Finding the singularity of the right-hand side (rhs) in Eq. (31) by solving  $\det[\tilde{\Pi}^{(\bar{p})}(\mathbf{q})] = 0$ , the dispersion  $\Omega_{\text{BS}}^{(\bar{p})}(\mathbf{q})$  of the BS is obtained. In general,  $\Omega_{\text{BS}}^{(\bar{p})}(\mathbf{q})$  has its minimum at  $\mathbf{q} = 0$ , and we refer to  $\Omega_{\text{BS}} \equiv \Omega_{\text{BS}}^{(\bar{p})}(\mathbf{0})$  as the gap of BS mode.

In the eSC state, we show that  $[\tilde{\Pi}^{(o)}(\Omega)]_{12}$  and  $[\tilde{\Pi}^{(o)}(\Omega)]_{21}$  are vanishingly small, and  $[\tilde{\Pi}^{(o)}(\Omega)]_{11}$  is finite in Appendix E. Thus, the zero of  $\det[\tilde{\Pi}^{(o)}(\Omega)] \approx [\tilde{\Pi}^{(o)}(\Omega)]_{11} [\tilde{\Pi}^{(o)}(\Omega)]_{22}$  is largely identical to the zero of  $[\tilde{\Pi}^{(o)}(\Omega)]_{22}$ , and the BS mode can be found by looking into the inverse of  $[\tilde{\Pi}^{(o)}(\Omega)]_{22}$ . Figure 3(a) shows  $\text{Im}[1/[\tilde{\Pi}^{(o)}(\Omega)]_{22}]$  in the eSC state at the zero-field over varying  $g_o/g_e$ . The gap of the BS mode  $\Omega_{\text{BS}}$  is clearly identified. Increasing  $g_o/g_e$  drops  $\Omega_{\text{BS}}$ , and  $\Omega_{\text{BS}}$  becomes zero at the critical ratio  $r_c = g_{o,c}/g_e \sim 1.21$  and disappears for larger  $g_e/g_o$ .

To relate the gap of the BS mode  $\Omega_{\text{BS}}$  with the stability of the superconducting ground state against the other pairing channel, we first derive a semi-analytical expression for  $\Omega_{\text{BS}}$  which is given by

$$\frac{2y \arcsin y}{\sqrt{1-y^2}} = \frac{1}{g_o N_{\text{tot}} \langle \sin^2 \chi \rangle_{\text{FS}}} - \frac{1}{g_e N_{\text{tot}}}, \quad (32)$$

where  $y = \Omega_{\text{BS}}/2\Delta_e$ , and  $N_{\text{tot}} = N_1 + N_2$  with  $N_{i=1,2}$  being the density of states of the  $i$ -th Fermi surface given by  $\xi_i = 0$ . [The total density of states is  $2N_{\text{tot}}$  due to the Kramers' degeneracy.] Here,  $\langle \dots \rangle_{\text{FS}} =$

$\sum_{i=1}^2 N_i \langle \dots \rangle_{\text{FS},i} / (N_1 + N_2)$  with  $\langle \dots \rangle_{\text{FS},i}$  being the angular average over the  $i$ -th Fermi surface [For the derivation, see Appendix E].

The rhs of Eq. (32) can be related with the superconducting phase transition temperatures if we note that, in the weak-coupling limit, the phase transition temperatures for the eSC state and the preempted oSC state are given by  $g_e N_{\text{tot}} = -1/\ln(T_{c,e}/\Lambda)$  and  $\langle \sin^2 \chi \rangle g_o N_{\text{tot}} = -1/\ln(T_{c,o}/\Lambda)$ , respectively, where  $\Lambda$  is a cutoff. Substituting these formulae to Eq. (33), we obtain a simple relation between  $\Omega_{\text{BS}}$  and  $T_{c,o}/T_{c,e}$ :

$$\frac{2y \arcsin y}{\sqrt{1-y^2}} = -\ln \frac{T_{c,o}}{T_{c,e}}. \quad (33)$$

Note that a real solution  $y$  exists as long as  $T_{c,o} \leq T_{c,e}$ , while it ceases to exist as soon as  $T_{c,o} > T_{c,e}$ . This implies that  $\Omega_{\text{BS}} = 0$  is an indication of the phase transition between two superconducting states.

Although Eq. (33) is derived by assuming the weak-coupling limit, let us make use of it to estimate  $\Omega_{\text{BS}}$  in  $\text{CeRh}_2\text{As}_2$  at the zero-field. Adopting  $T_{c,o}/T_{c,e} = 0.87$  which is estimated for  $\text{CeRh}_2\text{As}_2$  in Ref. [13], we find  $\Omega_{\text{BS}} \sim 0.51\Delta_e$ . Therefore, the BS mode in  $\text{CeRh}_2\text{As}_2$  may be expected to exist below the midst of the superconducting quasiparticle excitation gap, which is a favorable condition to discern the signature of the BS mode from the contributions from the quasiparticle excitations. It should be stressed that this estimation of  $\Omega_{\text{BS}}$  from Eq. (33) has nothing to do with our choice of the parameters such as  $t$ ,  $\mu$ ,  $\alpha_{\text{R}}$  for the normal phase Hamiltonian; it is a model-independent result under weak-coupling assumption.

In Fig. 3(b), the intensity of the BS mode peaks in  $\text{Im}[1/[\tilde{\Pi}^{(o)}(\Omega)]_{22}]$  is drawn for several  $g_o/g_e$  around the critical point. As the critical point is approached, the intensities of the peaks raise. The relation between  $\Omega_{\text{BS}}$  and the inverse of the peak height is shown in the inset which clearly reveals that the peak height is proportional to  $\Omega_{\text{BS}}^{-1}$  for small  $\Omega_{\text{BS}}$ .  $\text{Im}[1/[\tilde{\Pi}^{(e)}(\Omega)]_{22}]$  in the oSC state exhibits qualitatively identical trend except that the BS mode appears when  $g_o > g_{o,c}$ .

It should be remarked that  $\text{peak} \propto \Omega_{\text{BS}}^{-1}$  is a consequence of generic properties of the linear response kernel  $\tilde{\Pi}^{(o)}(-\Omega) = [\tilde{\Pi}^{(o)}(\Omega)]^\dagger$  [38] which ensures that  $\det \tilde{\Pi}^{(o)}(\Omega)$  is a real even function of  $\Omega$  for  $\Omega < 2\Delta_e$ . Therefore,  $\det \tilde{\Pi}^{(o)}(\Omega) \propto \Omega_{\text{BS}}^2 - \Omega^2$  when  $\Omega_{\text{BS}}$  and  $\Omega$  are small. Provided that  $\det \tilde{\Pi}^{(o)}(\Omega)$  and  $[\tilde{\Pi}^{(o)}(\Omega)]_{22}$  are proportional, we know  $\text{Im}[1/[\tilde{\Pi}^{(o)}(\Omega)]_{22}] \propto \delta(\Omega_{\text{BS}}^2 - \Omega^2) \propto \delta(\Omega_{\text{BS}} - \Omega)/\Omega_{\text{BS}}$ , and thus the intensity of the BS mode increases as  $\Omega_{\text{BS}}$  approaches to zero even when magnetic fields are applied. The same argument applies to the BS mode in the oSC state.

### C. Bardasis-Schrieffer mode under $B_z$

Figures 4(a) and 4(b) show the imaginary part of the inverse of the relevant component in  $\tilde{\Pi}^{(\bar{p})}(\Omega^+)$  in the pSC

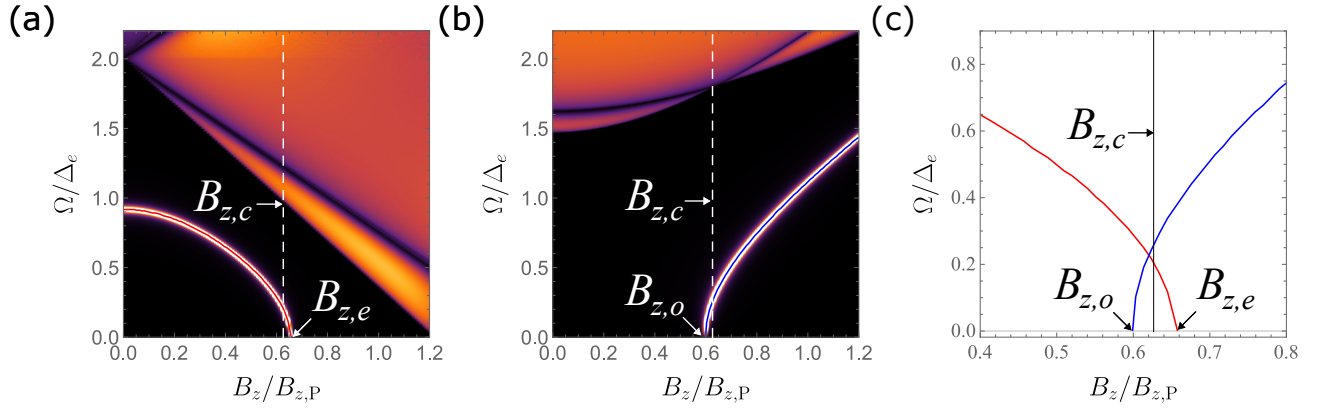


Figure 4. (a) False color plot of  $\text{Im}[1/\tilde{\Pi}^{(o)}(\Omega)]_{22}$  on the  $B_z - \Omega$  plane in the eSC state when  $g_o/g_e = 1.17$ . (b) False color plot of  $\text{Im}[1/\tilde{\Pi}^{(e)}(\Omega)]_{22}$  on the  $B_z - \Omega$  plane in the oSC state when  $g_o/g_e = 1.17$ . The vertical axes of both figures are normalized by the magnitude  $\Delta_e$  of the gap function in eSC state, while the horizontal axes are normalized by the Pauli magnetic field  $B_{z,P}$  of the eSC state. The vertical dashed lines in (a) and (b) mark the critical magnetic field at which the even-to-odd transition occurs. The critical magnetic field is obtained from Fig. 2(a). For (b),  $\Delta_o = 0.001$  is used. A rather larger  $\epsilon = 10^{-4}$  in  $\Omega^+$  is used exceptionally for (c) to avoid the numerical issues concerning the extremely sharp peaks.

state for  $\mathbf{B} = B_z \hat{z}$ . Here,  $g_o = 1.17g_e$  is used to make the features of figures easily recognizable. The reddish region of each figure represents the BdG quasiparticle excitations. Below the quasiparticle continuum, the curves corresponding to the gap of the BS mode  $\Omega_{\text{BS}}(B_z)$  in each  $p$ SC is clearly depicted. The red and blue lines are drawn over the curves for a guide to the eye. The vertical dashed lines in both figures denote the even-to-odd critical fields  $B_{z,c}$  identified in Fig. 2(a).

It is clearly seen that  $\Omega_{\text{BS}}(B_z)$  in eSC (oSC) phase is lowered as the external magnetic fields increase (decrease). This is consistent with the behavior of the BdG quasiparticle excitation gap. Also, it has to be noted that  $\Omega_{\text{BS}}(B_{z,c})$  is finite, while it becomes zero at  $B_z = B_{z,e} > B_{z,c}$  and  $B_z = B_{z,o} < B_{z,c}$  in eSC and oSC phases, respectively. Recalling that the eSC and oSC phases are the equilibrium ground states in  $B_z < B_{z,c}$  and  $B_z > B_{z,c}$ , respectively, the softening of those collective modes occurs outside the thermodynamic equilibrium [35]. Understood as a precursor of an instability of a state,  $B_{z,e}(B_{z,o})$  could be understood as the boundary to which the eSC(oSC) state can persist to exist as a metastable state. Therefore, if the experimentally observed hysteresis [13] may originate from the metastable eSC and oSC states, it is expected that the BS mode is almost gapless at the boundaries of the hysteresis curve.

As explained before, the peak height of the BS mode increases as the gap of the BS mode decreases.

#### IV. LINEAR OPTICAL RESPONSE IN LNCS SUPERCONDUCTOR

Thus far, we have demonstrated that the gap of the BS mode from the pairing channel with opposite parity to the ground state is lowered near the even-to-odd phase

transition and becomes gapless at a critical point which may be identified with a boundary of the hysteresis. In this section, we study the linear optical response from the BS mode.

The linear optical response incorporating the effect of the sub-dominant pairing fluctuation is derived from  $\mathcal{J}_i(q)/|e| = \delta S_{\text{eff}}/\delta \mathcal{A}_i(-q)$  with  $S_{\text{eff}}$  in Eq. (24):

$$\mathcal{J}_i(q)/|e| = K_{ij}(q)\mathcal{A}_j(q) + L_{ia}^{(\bar{p})}(q)\eta_a(q). \quad (34)$$

Substituting Eq. (31) into Eq. (34), we have  $\mathcal{J}_i(q)/|e| = \tilde{K}_{ij}(q)\mathcal{A}_j(q)$  with

$$\tilde{K}(q) = K(q) - L^{(\bar{p})}(q)[\tilde{\Pi}^{(\bar{p})}]^{-1}R^{(\bar{p})}(q), \quad (35)$$

where the second term in the rhs of Eq. (35) includes the contribution from the BS mode. Therefore, the BS mode would be detected as a peak in the optical absorption spectrum unless  $L_{ia}^{(\bar{p})}(\Omega)$  and  $R_{aj}^{(\bar{p})}(\Omega)$  are zero.

##### A. Multiband-assisted optical transition and non-zero $L^{(o)}$ and $R^{(o)}$

$L_{ia}^{(\bar{p})}(\Omega)$  and  $R_{aj}^{(\bar{p})}(\Omega)$  are frequently overlooked in literature. A partial reason for this may come from the conventional wisdom that the matrix elements of the velocity operators vanishes in the BCS model for the conventional superconductivity with a single electronic band [39] as we show explicitly below.

Unlike the conventional models for the trivial superconductivity with a single band normal phase Hamiltonian, however, the presence of multiple electronic bands can render  $L_{i,a}^{(\bar{p})}(\Omega)$  and  $R_{a,j}^{(\bar{p})}(\Omega)$  finite [40]. To emphasize the role of the multiple electronic bands, we provide a detailed analysis of  $L_{ia}^{(o)}(\Omega)$  and  $R_{aj}^{(o)}(\Omega)$  in this section

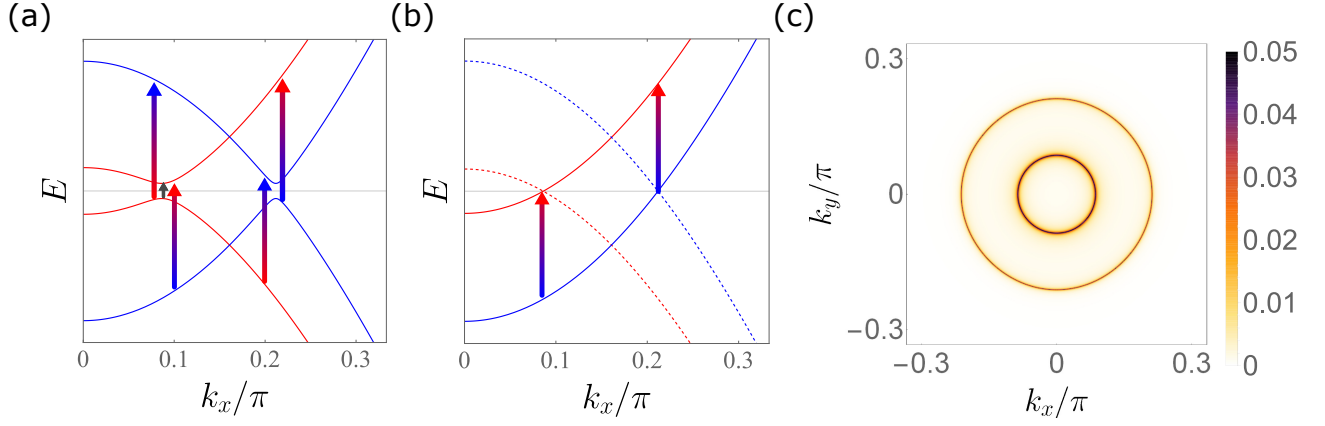


Figure 5. The band structure of (a)  $H_{\text{BdG}}$  in Eq. (11) and (b)  $H_0$  in Eq. (1). The gray arrows in (a) correspond to the forbidden optical transitions due to the vanishing matrix elements of the velocity operator  $\mathcal{V}_z$ . The arrows with color gradient indicate the optical transition making  $L_{z,2}^{(o)}$  and  $R_{2,z}^{(o)}$  finite.  $\Delta_e = 0.05$  are used for (a) and (b). (c) False color plot for the integrand  $F(\mathbf{k}, 0)$  of  $L_{z,2}^{(o)}$  with  $\Delta_e = 0.004$ .

based on the analytical expressions of them in the eSC state.

As shown in Appendix A, the spatial symmetries of  $H_0$  allow  $L_{z,2}^{(o)}$  to be finite whereas  $L_{x,2}^{(o)}$  and  $L_{y,2}^{(o)}$  are forbidden. Also, as  $L_{z,2}^{(o)}(\Omega) = [R_{2,z}^{(o)}(\Omega)]^*$ , we focus on  $L_{z,2}^{(o)}(\Omega)$ . The spectral representation of  $L_{z,2}^{(o)}$  is written down as

$$L_{z,2}^{(o)}(\Omega) = \frac{1}{2} \sum_{\mathbf{k}} \sum_{m,n} \frac{\langle m | \mathcal{V}_z | n \rangle \langle n | \tau_y \sigma_z | m \rangle}{\Omega^+ - E_m + E_n} \Theta_{mn}, \quad (36)$$

where the momentum dependence of the eigenstate  $|m\rangle$  and energy  $E_m$  are omitted.  $\Theta_{mn} \equiv \Theta(E_m) - \Theta(E_n)$  with the Heaviside step function  $\Theta(x)$ . The eigenenergies of  $H_{\text{BdG}}^{(e)}$  given by  $E_{c(v),i} = \pm \sqrt{\xi_i^2 + \Delta_e^2}$  for  $i = 1, 2$ . The corresponding eigenvectors are

$$\begin{aligned} |c, i, \alpha(\beta)\rangle &= \begin{pmatrix} \cos \frac{\Xi_i}{2} |\xi_i, \alpha(\beta)\rangle \\ \sin \frac{\Xi_i}{2} |\xi_i, \alpha(\beta)\rangle \end{pmatrix}, \\ |v, i, \alpha(\beta)\rangle &= \begin{pmatrix} -\sin \frac{\Xi_i}{2} |\xi_i, \alpha(\beta)\rangle \\ \cos \frac{\Xi_i}{2} |\xi_i, \alpha(\beta)\rangle \end{pmatrix}, \end{aligned} \quad (37)$$

with  $e^{i\Xi_i} = (\xi_i + i\Delta_e)/E_{c,i}$ .

Let us first evaluate the matrix elements of the velocity operator  $\mathcal{V}_z$   $\langle m | \mathcal{V}_z | n \rangle$  using Eqs. (37), (10a), and (10b). The elements  $\langle m | \mathcal{V}_z | n \rangle$  relevant to calculating  $L_{z,2}^{(o)}$  at the zero-temperature are given by

$$\langle c, i, \alpha | \mathcal{V}_z | v, j, \alpha' \rangle = \sin \frac{\Xi_i - \Xi_j}{2} \langle i, \alpha | \partial_z H_0 | j, \alpha' \rangle. \quad (38)$$

Note that the rhs is zero when  $i = j$ . These elements correspond to the forbidden transitions  $\langle c, i, \alpha | \mathcal{V}_z | v, i, \alpha \rangle$  that are marked by gray arrows in Figure 5(a), where the energy bands of the BdG quasiparticles are drawn. Furthermore, an explicit calculation using the eigenvectors in Eqs. (10a) and (10b) shows that  $\langle i, \alpha | \partial_z H_0 | j, \alpha' \rangle \propto \delta_{\alpha\alpha'}$ .

Therefore, only  $\langle c, 1, \alpha | \mathcal{V}_z | v, 2, \alpha \rangle$  and the other elements related to this by the complex conjugation or a replacement  $1 \leftrightarrow 2$  or  $\alpha \leftrightarrow \beta$  are finite. The arrows with color gradient in Fig. 5(a) represent the transitions related to these finite elements of the velocity operator. Comparing it to the electronic band structure in the normal phase displayed in Fig. 5(b), these finite transitions can be understood as the remnants of the interband transitions in the normal phase which are marked by arrows in Fig. 5(b).

To calculate  $L_{z,2}^{(o)}(\Omega)$ , we further need to evaluate  $\langle c, 2, \alpha | \tau_y \sigma_z | v, 1, \alpha \rangle$  which is given by

$$\langle c, 2, \alpha | \tau_y \sigma_z | v, 1, \alpha \rangle = \frac{e^{i(\zeta+\phi)} t_{\mathbf{k}} \cos \chi}{2i} \cos \frac{\Xi_2 - \Xi_1}{2}, \quad (39)$$

and the other elements related to it by the complex conjugation or the replacement  $1 \leftrightarrow 2$  are also finite.

Substituting Eqs. (38) and (39) into Eq. (36) results in

$$L_{z,2}^{(o)}(\Omega) = - \int F(\mathbf{k}, \Omega) d^d \mathbf{k} / (2\pi)^d, \quad (40)$$

$$F(\mathbf{k}, \Omega) = \frac{(E_{c,1} + E_{c,2}) t(\mathbf{k}) \cos \chi \sin(\Xi_2 - \Xi_1)}{(E_{c,1} + E_{c,2})^2 - (\Omega^+)^2}. \quad (41)$$

Note that the possible singularities of  $F(\mathbf{k}, \Omega)$  are located at  $|\Omega| = \Delta_e + |\xi_{1,\mathbf{k}} - \xi_{2,\mathbf{k}}|$  which are fairly distant from the region of interest  $|\Omega| < 2\Delta_e$ . Hence, it is a good approximation to set  $\Omega = 0$  in Eq. (41). We draw  $F(\mathbf{k}, 0)$  in Fig. 5(c).  $F(\mathbf{k}, 0)$  has narrow positive peaks around the Fermi surfaces like the integrands that are commonly encountered in the weak-coupling theory of superconductivity. Around each Fermi surface,  $F(\mathbf{k}, 0) \approx \frac{\Delta_e \cos^2 \chi}{4E_i(\mathbf{k})}$ , and thus

$$L_{z,2}^{(o)}(\Omega) \approx - \sum_{\mathbf{k}} \frac{\Delta_e \cos^2 \chi}{4E_i} = - \frac{\Delta_e \langle \cos^2 \chi \rangle_{\text{FS}}}{2g_e}. \quad (42)$$



where we use the BCS gap equation  $1/g_e = (N_1 + N_2) \int d\xi (\xi^2 + \Delta_e^2)^{-1/2}$  with  $N_i$  the density of states of the  $i$ -th Fermi surface given by  $\xi_i = 0$ . Though  $\Delta_e/g_e$  is small,  $L_{z,2}^{(o)}(\Omega)$  is finite as long as  $\langle \cos^2 \chi \rangle_{\text{FS}} \neq 0$ , which is proportional to the square of interlayer hopping  $t_c^2$ . Also, we can know that  $L_{z,2}^{(o)}(\Omega)$  decreases as  $\alpha_{\text{R}}^2$  increases from Eq. (42) as  $N_{\text{tot}}$  converges to a constant proportional  $1/t$ . For the estimation of  $L_{z,2}^{(o)}$  under the weak-coupling assumption with  $g_o = g_e$ , see Appendix. D.

### B. Optical response under $B_z$

Provided that the fluctuation in the subdominant pairing channel is linearly coupled to the light, the behavior of the gaps of the BS modes around the even-to-odd transition can be investigated through an optical measurement in the linear response regime. Figures 6(a) and 6(b) show the imaginary part of the linear response kernel  $\tilde{K}_{zz}(\Omega)$  in Eq. (35) for varying  $B_z$  in the eSC and the oSC states, respectively, with  $g_o = 1.17g_e$ . It is easy to see the signature from the collective modes appearing in  $\text{Im}[1/\tilde{\Pi}_{22}^{(\bar{p})}(\Omega)]$  in Figs. 4(a) and 4(b). Also, the BS mode is well separated from the BdG quasiparticle pair-breaking continuum. Since  $L_{z,a}^{(\bar{p})}(\Omega)$  is finite far below the pair-breaking continuum, it lets the collective modes make distinguished contributions to  $\text{Im}[\tilde{K}_{zz}(\Omega)]$ . At the point where the gap of the BS mode vanishes, the peak intensity of the BS modes diverges and  $\text{Im}[\tilde{K}_{zz}(\Omega)]$  exhibits the strongest peak from the BS mode. Thus, the absorption peak in the optical response measurement is expected to be strongest at the boundaries of the hysteresis curve around the even-to-odd transition.

Figs. 6(d)~(f) shows  $\text{Im}[\tilde{K}_{zz}(\Omega)]$  and  $L_{z,2}^{(\bar{p})}$  when  $g_o = g_e$ . Unlike Fig. 6(a), Fig. 6(d) is featured by that the pair-breaking continuum is around the  $\Omega = 0$  line when  $\Omega_{\text{BS}} \sim 0$ . Because of the lowered pair-breaking continuum, the magnitude of  $L_{z,2}^{(o)}(\Omega)$  is diminished as  $B_z$  increases. Fig. 6(f) explicitly shows how  $L_{z,2}^{(o)}(\Omega)$  changes with  $B_z$ . For magnetic fields close to either of  $B_{z,e}$  and  $B_{z,o}$  at which  $\Omega_{\text{BS}}$  vanishes, the magnitude of  $L_{z,2}^{(\bar{p})}(\Omega)$  rapidly drops off. The diminished  $L_{z,a}^{(\bar{p})}(\Omega)$  enfeebls the intensity of the peak at  $\Omega = \Omega_{\text{BS}}$ . Especially when  $g_o = g_e$ , the magnetic field  $B_z$  rendering  $L_{z,2}^{(\bar{p})}(0) = 0$  coincides with the magnetic field at which  $\Omega_{\text{BS}} = 0$  occurs. Subsequently, the gapless BS mode from the  $\bar{p}$ -parity pairing channel in  $p$ SC seems to have no effect on the linear optical response in this limit because the coupling  $L_{z,2}^{(\bar{p})}$  between the BS mode and the light vanishes.

However, this exact coincidence of  $\Omega_{\text{BS}} = 0$  and  $L_{z,a}^{(\bar{p})} = 0$  under the out-of-plane magnetic field is an unavoidable consequence of symmetry. It turns out that the coincidence happens to occur because we ignore the Ising-type spin-orbit coupling  $\lambda_{\text{I}}$ , which results in  $F_A(\mathbf{k}) \equiv [\sigma_z, H_0(\mathbf{k})]/4i = \mathcal{V}_z(\mathbf{k})$ . Without  $\lambda_{\text{I}}$ , the

zero-frequency response kernel  $\tilde{\Pi}_{22}^{(\bar{p})}$  is given by

$$\tilde{\Pi}_{22}^{(\bar{p})}(0) = \frac{1}{g_o} - \frac{1}{g_e} - \frac{\sum_{\mathbf{k}} \text{Tr}[\tau_y^{(o)} G(\mathbf{k}) F_A(\mathbf{k}) G(\mathbf{k})]}{\Delta_p} \quad (43)$$

$$= \frac{1}{g_o} - \frac{1}{g_e} - \frac{2L_{z,2}^{(\bar{p})}(0)}{\Delta_p}. \quad (44)$$

where we use  $F_A(\mathbf{k}) = \mathcal{V}_z(\mathbf{k})$  in the second line. Given  $g_o = g_e$ , the rhs is zero when  $L_{z,2}^{(\bar{p})}(0) = 0$ . Adding the Ising-type spin-orbit coupling forces  $F_A(\mathbf{k}) \neq \mathcal{V}_z(\mathbf{k})$  and enables the gapless BS mode contribute to the linear optical response in principle.

## V. SUMMARY AND DISCUSSION

We have investigated the BS modes from an odd- and even-parity pairing channels in the eSC and oSC state, respectively, by using a generic model for locally non-centrosymmetric superconductors involving two orbital degrees of freedom. Our result based on the GRPA shows the gap of the BS mode in the eSC (oSC) state is lowered with the increasing (decreasing) out-of-plane magnetic field and eventually becomes gapless. Since the softening of the BS modes is the precursor of the end of the metastability of a superconducting state, we deduce that the softening should occur at the boundaries of the hysteresis curve around the first order even-to-odd transition.

As the BS modes considered in this work originate from the pairing channels with the parity opposite from that of the ground state pairing, there can be a finite linear coupling between the light and the BS modes. We have demonstrated that the linear coupling is indeed finite due to the presence of the multiple electronic bands, which can be thought of as an intrinsic characteristic of a locally non-centrosymmetric system with two orbital degrees of freedom in the primitive cell. Therefore, we look forward that the signature of the collective mode can be observed by measuring the linear optical response, especially in the microwave regime, of CeRh<sub>2</sub>As<sub>2</sub> for which  $\Omega_{\text{BS}} \sim 0.51\Delta_e$  is expected at the zero-field.

It should be stressed that the detection the BS modes via an *linear* optical response measurement is a smoking gun signature from the bulk of CeRh<sub>2</sub>As<sub>2</sub> evidencing the competing odd-parity pairing channel. This is because the linear optical coupling is possible only when the dominant and the sub-dominant pairing channels are opposite in parity. Moreover, as exposed in Appendix A, the light selectively couples to a particular set of odd-parity pairings. Put into the group theoretical jargon, only the pairing channels belonging to the irreducible representations of  $\mathbf{J}_i$  are able to affect the optical response in the linear response regime. Therefore, the detection of the BS modes not only can be taken as a compelling proof, i.e. sufficient, for the existence of the odd-parity pairing channel, but also can place restrictions on the form of

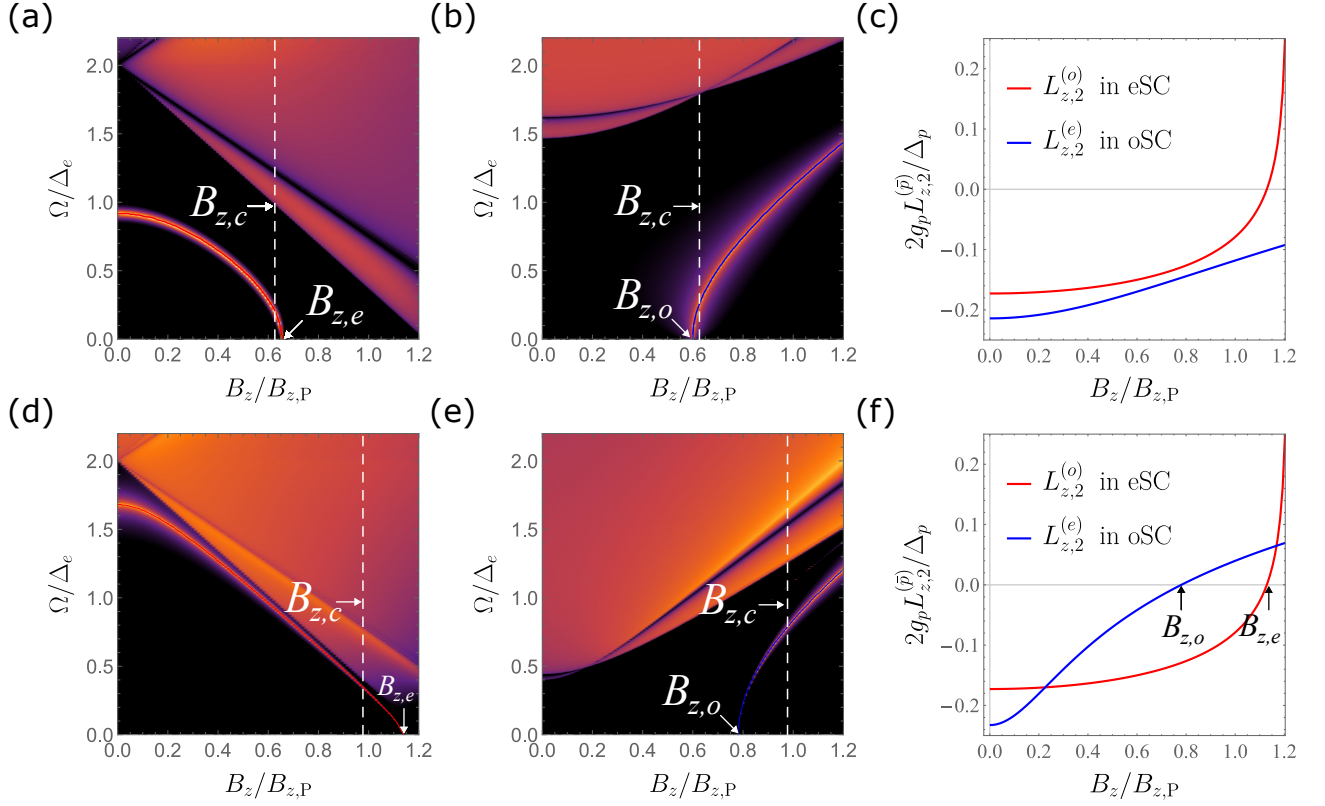


Figure 6. False color plots for  $\text{Im}[\tilde{K}_{zz}(\Omega)]$  on the  $B_z - \Omega$  plane. For (a), (b), and (c),  $g_o/g_e = 1.17$  is used, while (d), (e) and (f) are calculated with  $g_o/g_e = 1$ . (a) and (d)  $\text{Im}[\tilde{K}_{zz}(\Omega)]$  in the eSC state, (b) and (e)  $\text{Im}[\tilde{K}_{zz}(\Omega)]$  in the oSC state. (c) and (f)  $L_{z,2}^{(\bar{p})}(\Omega)$  of both phases normalized by  $g_p/2\Delta_p$ . The red and blue lines correspond to  $L_{z,2}^{(o)}(\Omega)$  in the eSC state and  $L_{z,2}^{(e)}(\Omega)$  in the oSC state, respectively.

the odd-parity pairing channels. It also deserves to be noted that the gap of the BS mode in the oSC increases with increasing out-of-plane magnetic field. This feature may be regarded as a proof of the parity-switching at the first order transition in the superconducting phase of  $\text{CeRh}_2\text{As}_2$  because the gap of the BS mode should decrease if it were not for the parity-switching.

Though the Pauli paramagnetic depairing is considered as the primary cause of the first order transition in the superconducting state of  $\text{CeRh}_2\text{As}_2$ , our findings and argument are applicable to any superconducting systems exhibiting parity-switching transitions between two superconducting states regardless of the underlying mechanism and the transition order. An interesting application is the superconductivity in a system hosting a structural instability [9, 11, 12, 41] e.g. ferroelectric instability. We address the cases in the two perspectives. Firstly, if the even-to-odd transition is realized within the centrosymmetric state of this system, it is possible to have a soft BS mode at the transition, which may also be observed in an optical response measurement in the linear response regime. Also, by noting that the topological characterization of the superconductor can accompany the transition, both of the fermionic and the collective excitations are gapless at the transition and thus an intriguing phenom-

ena such as the non-Fermi liquid state could be brought about.

The second case is when such a transition occurs in the non-centrosymmetric state. In this case, the superconducting phase could host an intriguing topological phase transition between an even-parity dominant trivial superconductivity and an odd-parity dominant topological superconductivity, and a low-lying Leggett mode could appear at the transition [11, 12]. The existence of such a topological phase transition implies there are at least two competing pairing channels whose parities were opposite if it were not for the inversion-breaking order. However, the inversion-breaking order blurs the sharp distinction between even- and odd-parity pairings, which could lead both pairing channels to belonging to the same irreducible representation of the symmetry group of the state. In such a case, the BS mode from the competing pairing channel will turn into a Leggett mode, which is discussed in Refs [11, 12]. This Leggett mode can also be coupled linearly to the light due to the absence of the inversion symmetry [40].

Lastly, a recent experiments suggests that the possibility of an inversion-breaking antiferromagnetic order coexisting with superconductivity in  $\text{CeRh}_2\text{As}_2$  [34, 42]. As the presence of the antiferromagnetic order can reduce

the group of the symmetries of the system, its potential effect on the existence of BS modes and influence on the optical measurement calls for further investigation.

## ACKNOWLEDGMENTS

We express our sincere thanks to Nico A. Hackner and P. M. R. Brydon for generously sharing their unpublished preprint on the BS mode [43]. We also thank Daniel Agterberg, Hongki Min, Yunsu Jang, Jiho Jang, and Sungmo Kang for helpful discussions. S.B.C. was supported by the National Research Foundation of Korea (NRF) grants funded by the Korea government (MSIT) (2020R1A2C1007554) and the Ministry of Education (2018R1A6A1A06024977).

### Appendix A: The other odd-parity channels

#### 1. When the ground state at the zero-field is an even-parity state

In this section, we discuss the linear coupling between the other odd parity channels and the light (or the current). We first note that the presence of an inversion  $\mathcal{I} = \sigma_x$  and a time-reversal symmetry  $\mathcal{T} = is_y\mathcal{K}$  enforces for the normal phase Hamiltonian to take the following form

$$H_0(\mathbf{k}) = \varepsilon_{00}(\mathbf{k})\sigma_0s_0 + (\varepsilon_{10}(\mathbf{k})\sigma_x + \varepsilon_{20}(\mathbf{k})\sigma_y)s_0 + \sigma_z(\varepsilon_{31}(\mathbf{k})s_x + \varepsilon_{32}(\mathbf{k})s_y + \varepsilon_{33}(\mathbf{k})s_z) \quad (\text{A1})$$

where  $\varepsilon_{00}(\mathbf{k})$  and  $\varepsilon_{10}(\mathbf{k})$  are even functions under  $\mathbf{k} \rightarrow -\mathbf{k}$  while  $\varepsilon_{20}(\mathbf{k})$  and  $\varepsilon_{3i}(\mathbf{k})$  are odd functions. The linear coupling between a pairing channel and the light is possible only when a pairing channel transforms like one of the current operators  $J_i$  under the symmetries of  $H_0(\mathbf{k})$ . For CeRh<sub>2</sub>As<sub>2</sub>, the point group  $D_{4h}$  is the symmetry of the Hamiltonian at  $\Gamma$  in the Brillouin zone. By using the symmetries of the point group  $D_{4h}$ , we analyze the selection rule for odd-parity channels transforming like either of  $k_x s_y - k_y s_x$ ,  $k_z s_z$ ,  $k_z \sigma_x s_z$  and  $k_x s_x + k_y s_y$  which are discussed in Refs. [33].

Table I summarizes the parities of the current operators and the form factors of those odd-parity channels under several two-fold transformations. The signs tell whether  $TO(\mathbf{k})T^{-1} = +O(T\mathbf{k})$  or  $TO(\mathbf{k})T^{-1} = -O(T\mathbf{k})$  where  $O$  represents one of the currents or the form factors in the first column of the Table I and  $T$  represents a symmetry transformation in the first row of the table.

Firstly, the linear coupling between the in-plane currents  $J_x$  and  $J_y$  and the odd-parity gap functions in Table I is forbidden by, for example,  $C_{2z}$ . It is easy to see that the odd-parity channel transforming like  $k_x s_x + k_y s_y$  or  $k_z s_z$  can not be linearly coupled to the light because of  $C_{2z}$  and  $C_{2x}$ . The odd-parity channel labeled by

	$\mathcal{I} (\sigma_x)$	$C_{2z} (s_z)$	$C_{2x} (\sigma_x s_x)$	$\mathcal{A} (\sigma_y s_x \mathcal{K})$
$J_z, \sigma_z$	−	+	−	−
$\{J_x, J_y\}$	−	−	$\{+, -\}$	−
$k_x s_y - k_y s_x$	−	+	−	+
$k_z s_z$	−	+	+	−
$k_x s_x + k_y s_y, k_z \sigma_x s_z$	−	+	+	+

Table I. Character table for some two-fold and  $M_{(abc)}$  is a mirror operation against a plane perpendicular to the vector  $(a, b, c)$ .  $C_{(110)}$  is a two-fold rotation around the axis  $(1, 1, 0)$ . Here,  $\mathbf{\Omega} = \hat{\mathbf{n}}_{110} \cdot \mathbf{s}$ .

$k_x s_y - k_y s_x$  transforms like  $J_z$  for all two-fold symmetries in  $D_{4h}$ . Indeed,  $J_z$  and  $k_x s_y - k_y s_x$  belong to the same irreducible representation, and thus  $k_x s_y - k_y s_x$  can be coupled to the light as  $\sigma_z$  can.

In the above symmetry-based analysis, however, the details of the electronic structure is not taken into consideration. For CeRh<sub>2</sub>As<sub>2</sub>, the large contribution to  $\varepsilon_{33}(\mathbf{k})$  may be supposed to originate from the Ising-type spin-orbit couplings between next-nearest-neighbor Ce atoms. As long as this Ising-type spin-orbit coupling is so negligible that  $\varepsilon_{33}$  is also negligible compared to other  $\varepsilon_{ij}$ , we can show that the coupling between  $k_x s_y - k_y s_x$  and  $J_z$  is much smaller than that between  $\sigma_z$  and  $J_z$ .

To prove it, we first note that the non-trivial part of the normal phase Hamiltonian  $\tilde{H}_0(\mathbf{k}) \equiv H_0(\mathbf{k}) - \varepsilon_{00}(\mathbf{k})\sigma_0s_0$  possesses an additional *antiunitary antisymmetry*  $\mathcal{A} = U_A\mathcal{K}$  of  $\tilde{H}_0(\mathbf{k})$  with  $U_A = is_y s_x$ . It transforms under  $\mathcal{A}$  as  $U_A\tilde{H}_0(\mathbf{k})^*U_A^\dagger = -\tilde{H}(\mathbf{k})$ . By  $\mathcal{A}$ , the eigenvectors  $|\xi_1, \alpha\rangle$  and  $|\xi_1, \beta\rangle$  are related to  $|\xi_2, \alpha\rangle$  and  $|\xi_2, \beta\rangle$ :

$$\mathcal{A}|\xi_1, \alpha\rangle = \sum_{\alpha'=\alpha, \beta} [\Gamma_A]_{\alpha', \alpha} |\xi_2, \alpha'\rangle, \quad (\text{A2})$$

$$\mathcal{A}|\xi_2, \alpha\rangle = \sum_{\alpha'=\alpha, \beta} [-\Gamma_A^T]_{\alpha', \alpha} |\xi_1, \alpha'\rangle, \quad (\text{A3})$$

where  $\Gamma_A$  is a  $2 \times 2$  unitary matrix. Here, we use  $U_A = -U_A^T$ .

The antiunitary antisymmetry of  $\tilde{H}_0$  is especially useful when the linear coupling is computed between the current operator  $J_z$  and the pairing fluctuations with the form factor  $M_{\mathbf{k}}$  in the eSC state with the trivial ground state gap function. In the calculation, we frequently encounter terms such as  $\mathcal{I}_{m\bar{m}} = \sum_{\alpha, \beta} \langle m, \alpha | J_z | \bar{m}, \beta \rangle \langle \bar{m}, \beta | M_{\mathbf{k}} | m, \alpha \rangle$  with  $\bar{m} = -m$  being 1 or 2, which determine the selection rule for the optical response. A tedious manipulation leads us to

$$\mathcal{I}_{m\bar{m}} = \lambda_{J_z} \lambda_M \mathcal{I}_{m\bar{m}}, \quad (\text{A4})$$

where  $\lambda_{\mathcal{O}}$  is the parity of the operator  $\mathcal{O}$  with respect to  $\mathcal{A}$ . Thus, if  $\lambda_{J_z} \lambda_M = -1$ , the linear coupling between the pairing fluctuation and the light characterized by the form factor  $M_{\mathbf{k}}$  is forbidden. In Table I, the parity of the form factors of the pairing channels are listed. Note

that both  $J_z$  and  $\sigma_z$  are odd under  $\mathcal{A}$  while  $k_x s_y - k_y s_x$  is even. Therefore, the linear coupling between the light and the fluctuation in the pairing channel  $k_x s_y - k_y s_x$  is negligible as long as the Ising-type spin-orbit coupling is negligible.

## 2. Both superconducting phases are odd-parity under inversion

In Ref. [21], it is proposed that the  $H - T$  phase diagram of the superconducting states of CeRh<sub>2</sub>As<sub>2</sub> might be reproduced with inter-layer spin-triplet odd-parity gap functions. There, the low-field state is characterized by an odd-parity spin-triplet gap function transforming like  $k_x k_y k_z (k_x^2 - k_y^2) \sigma_x s_z$  that belongs to  $A_{1u}$  of  $D_{4h}$ . The gap function of the high-field state is another odd-parity spin-triplet gap function transforming  $\sigma_y s_z$  belonging to  $A_{2u}$  of  $D_{4h}$ .

For this case, a BS mode should exist because both pairing channels belong to different irreducible representation. Since both pairing channels have the same inversion parity, the BS mode is inactive in the linear optical response.

## Appendix B: Odd-parity superconductivity in the in-plane magnetic fields

The behavior of the gap functions  $\Delta_e$  and  $\Delta_o$  under the in-plane magnetic field is exposed in detail here.

### 1. eSC phase under the in-plane magnetic field $B_x$

Using the basis diagonalizing  $H_0(\mathbf{k})$ , the BdG Hamiltonian in pSC is written as

$$U^\dagger H_{\text{BdG}}^{(e)} U = \tau_z \begin{pmatrix} \xi_1 & \\ & \xi_2 \end{pmatrix} + \Delta_e \tau_x + B_x U^\dagger s_x U, \quad (\text{B1})$$

$$U^\dagger s_x U = \begin{pmatrix} \hat{\mathbf{a}} \cdot \boldsymbol{\rho} & -i\rho_0 \cos \chi \sin \phi \\ i\rho_0 \cos \chi \sin \phi & -\hat{\mathbf{a}} \cdot \boldsymbol{\rho} \end{pmatrix}, \quad (\text{B2})$$

where

$$U = \frac{1}{\sqrt{2}} \tau_0 \otimes \begin{pmatrix} 1 & & & 1 \\ a & a^* e^{i\zeta} & -b & -b^* e^{i\zeta} \\ b & -b^* e^{i\zeta} & -a & a^* e^{i\zeta} \\ & e^{i\zeta} & & e^{i\zeta} \end{pmatrix}. \quad (\text{B3})$$

with  $a = e^{i\phi} \sin \chi$  and  $b = e^{i\zeta} \cos \chi$ . Here,  $\rho_i$  are the pseudospin Pauli matrices and  $\hat{\mathbf{a}} = (\cos \chi, 0, \sin \chi \cos \phi)$ . Assuming that  $|B_x| \ll |\xi_1 - \xi_2|$  at both Fermi surfaces, we can ignore the off-diagonal components of  $U^\dagger s_x U$  in the rhs of Eq. (B1). To gain a meaningful insight, we further introduce another unitary matrix  $U_a$  that diagonalizes  $\hat{\mathbf{a}} \cdot \boldsymbol{\rho}$ . Then, the BdG Hamiltonian  $U_a^\dagger U^\dagger H_{\text{BdG}}^{(e)} U U_a$  is

approximated by  $\bar{H}_{\text{BdG}}^{(e)}$  given by

$$\bar{H}_{\text{BdG}}^{(e)} = \tau_z \begin{pmatrix} \xi_1 & \\ & \xi_2 \end{pmatrix} + \mathbf{g} B_x \tau_0 \begin{pmatrix} \mu_z & \\ & -\mu_z \end{pmatrix} + \tau_x \Delta_e. \quad (\text{B4})$$

Here,  $\mu_i$  are the Pauli matrices the final basis and  $\mathbf{g} = \sqrt{\cos^2 \phi \sin^2 \chi + \cos^2 \chi}$  represents an effective Zeeman coupling in response to the in-plane magnetic field.

Note that  $\bar{H}_{\text{BdG}}^{(e)}$  is decomposed into four  $2 \times 2$  blocks which take the following form  $\pm \tau_0 \mathbf{g} B_x + \tau_z \xi_i + \tau_x \Delta_e$  whose eigenvalues are given by  $\pm B_x \mathbf{g} \pm \sqrt{\xi_i^2 + \Delta_e^2}$ . Direct manipulation of the self-consistent gap equation results in

$$\frac{1}{g_e} = \sum_{\mathbf{k}} \sum_i \frac{1}{2E_i} \sum_{s=\pm} \tanh \frac{\beta(E_i + s \mathbf{g} B_x)}{2}, \quad (\text{B5})$$

which is reduced to the following form at the zero-temperature

$$\frac{1}{g_e} = \sum_{\mathbf{k}} \sum_i \frac{\Theta(E_i - \mathbf{g} B_x)}{E_i}. \quad (\text{B6})$$

The Heaviside theta function appear because of the cancellation of the two tanh's in Eq. (B6). Indeed, this equation is exactly what explains the first-order transition by the Pauli pair-breaking in the conventional superconductors [18]. However, if  $B_x$  is increased so that  $B_x \min_{\phi}(\mathbf{g}) > \Delta_e$ , then a low-energy region  $|\xi_i| < \sqrt{B_x^2 \min_{\phi}(\mathbf{g}^2) - \Delta_e^2}$  is got rids of from the energy integration, which prevents us to obtain a finite  $\Delta_e$  as a solution of Eq. (B6) for small  $g_e$ . Figure. 7(a) shows  $\Delta_e$  which is obtained by numerically solving the self-consistent gap equation under the in-plane magnetic fields. It is easily recognized that  $\Delta_e$  discretely jumps to zero for strong  $B_x$ .

### 2. oSC phase under the in-plane magnetic field $B_x$

Using  $U$  in Eq. (B3), the oSC BdG Hamiltonian is transformed into

$$U^\dagger H_{\text{BdG}}^{(o)} U = \tau_z \begin{pmatrix} \xi_1 & \\ & \xi_2 \end{pmatrix} + U^\dagger \{ \Delta_o \tau_x \sigma_z + B_x s_x \} U, \quad (\text{B7})$$

where

$$U^\dagger \sigma_z U = \begin{pmatrix} \sin \chi \hat{\Sigma}_d \cdot \boldsymbol{\rho} & \cos \chi \hat{\Sigma}_{od} \cdot \boldsymbol{\rho} \\ \cos \chi \hat{\Sigma}_{od} \cdot \boldsymbol{\rho} & \sin \chi \hat{\Sigma}_d \cdot \boldsymbol{\rho} \end{pmatrix} \quad (\text{B8})$$

with  $\hat{\Sigma}_d = (\cos \chi \cos \phi, \cos \chi \sin \phi, \sin \chi)$  and  $\hat{\Sigma}_{od} = (-\sin \chi \sin \phi, -\sin \chi \cos \phi, \cos \chi)$ . Adopting the same assumptions used in analyzing the eSC phase, we neglect the off-diagonal blocks in  $U^\dagger \sigma_z U$  and  $U^\dagger s_x U$ . We also neglect the off-diagonal components in the diagonal blocks of  $B_x U^\dagger s_x U$ . The final BdG Hamiltonian that we use to address the behavior of  $\Delta_o$  under the in-plane magnetic field is given by

$$U^\dagger H_{\text{BdG}}^{(o)} U \approx \bar{H}_{\text{BdG}}^{(o)} = \begin{pmatrix} \xi_1 + \bar{B}_x \rho_z & & \Delta_o \sin \chi \hat{\Sigma}_d \cdot \boldsymbol{\rho} & \\ & \xi_2 - \bar{B}_x \rho_z & & \Delta_o \sin \chi \hat{\Sigma}_d \cdot \boldsymbol{\rho} \\ \Delta_o \sin \chi \hat{\Sigma}_d \cdot \boldsymbol{\rho} & & -\xi_1 + \bar{B}_x \rho_z & \\ & \Delta_o \sin \chi \hat{\Sigma}_d \cdot \boldsymbol{\rho} & & -\xi_2 - \bar{B}_x \rho_z \end{pmatrix} \quad (\text{B9})$$

$$= \begin{pmatrix} \xi_1 + \bar{B}_x \rho_z & \Delta_o \sin \chi \hat{\Sigma}_d \cdot \boldsymbol{\rho} \\ \Delta_o \sin \chi \hat{\Sigma}_d \cdot \boldsymbol{\rho} & -\xi_1 + \bar{B}_x \rho_z \end{pmatrix} \oplus \begin{pmatrix} \xi_2 + \bar{B}_x \rho_z & \Delta_o \sin \chi \hat{\Sigma}_d \cdot \boldsymbol{\rho} \\ \Delta_o \sin \chi \hat{\Sigma}_d \cdot \boldsymbol{\rho} & -\xi_2 + \bar{B}_x \rho_z \end{pmatrix} \quad (\text{B10})$$

with  $\bar{B}_x = B_x \cos \phi \sin \chi$ .

It is noteworthy that  $\bar{H}_{\text{BdG}}^{(o)}$ , contrasting to  $\bar{H}_{\text{BdG}}^{(e)}$ , involves a pairing between two bands of the same energy dispersion  $\xi_i \pm \sin \chi \cos \phi B_x$  through the off-diagonal component in  $\Delta_o \sin \chi \hat{\Sigma}_d \cdot \boldsymbol{\rho}$ . If it were not for the off-diagonal elements, the overall structure of  $\bar{H}_{\text{BdG}}^{(o)}$  would be identical to that of  $\bar{H}_{\text{BdG}}^{(e)}$  in Eq. (B4), and the oSC phase would exhibit a discontinuous transition to the normal phase at a strong enough  $B_x$ . The off-diagonal components in  $\Delta_o \sin \chi \hat{\Sigma}_d \cdot \boldsymbol{\rho}$  make the difference. Let us investigate their implication by neglecting the diagonal components completely. Under this assumption, the  $4 \times 4$  subblocks of  $\bar{H}_{\text{BdG}}^{(o)}$  is further decomposed into two  $2 \times 2$  subblocks of the form like

$$\begin{pmatrix} \xi_i + \sin \chi \cos \phi B_x & \Delta_o \cos \chi \sin \chi e^{i\phi} \\ \Delta_o \cos \chi \sin \chi e^{-i\phi} & -\xi_i - \sin \chi \cos \phi B_x \end{pmatrix}. \quad (\text{B11})$$

Note that  $B_x \sin \chi \cos \phi$  can be absorbed into  $\xi_i$  and thus the fully gapped superconductivity is retained for any  $g_o$  regardless of  $B_x$ .

The numerical results displayed in Fig. 7(b) confirm the analytical analysis. The green and orange lines represents solutions of the self-consistent gap equation, which are obtained by using  $\bar{H}_{\text{BdG}}^{(o)}$  without the diagonal and the off-diagonal components in the gap functions, respectively. With only the diagonal components in the gap function, a first-order transition to the normal phase appears, while the superconducting phase can robustly withstand against the in-plane magnetic fields when only the off-diagonal components are retained. The black solid line represents a solution of the self-consistent gap equation using  $H_{\text{BdG}}^{(o)}$  without any approximation. The solution shows an intriguing exponential decrease under  $B_x$ , which is a compromise between what the diagonal and off-diagonal components favor. Because of the exponential decrease which never touches the zero, the Pauli limiting field  $B_{x,P}$  in the oSC state is infinite at the zero temperature, which is in a sharp contrast to the eSC state. The gray dashed line is a solution of the self-consistent gap equation with  $H_{\text{BdG}}^{(o)}$  when the interlayer hopping  $t_c$  in  $H_0$  is set to a value much smaller than the gap function. In this 2D limit, the sign-alternating gap function  $\sigma_z$  is not discerned from the trivial gap function  $\sigma_0$  by the electrons. Thus, the oSC state also exhibits the first-

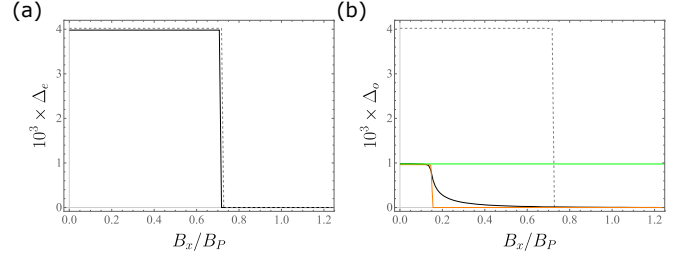


Figure 7. The evolution of the gap functions under the increasing in-plane magnetic fields. (a) The solid (dashed) line represent  $\Delta_e$  vs  $B_x$  when  $t_c = 0.1$  ( $t_c = 0$ ) is used in  $H_0$ . The  $t_c = 0$  case corresponds to the purely 2D case and largely coincides with the result in Ref. [44]. (b)  $\Delta_o$  vs  $B_x$  for several cases. The gray dashed line is obtained with  $t_c = 0.0005 \ll |\Delta_o|$  in  $H_0$ , which is qualitatively same with the dashed line in (a). The solid lines are obtained with  $t_c = 0.1 \gg |\Delta_o|$ . Of the three lines, the block line corresponds to a solution of the self-consistent gap equation when every terms in  $H_{\text{BdG}}^{(o)}$  are retained. The green and orange lines are the results calculated by using  $\bar{H}_{\text{BdG}}^{(o)}$  in Eq. (B10) neglecting the diagonal and the off-diagonal components in the gap function part, respectively.

order transition to the normal phase like as the eSC state does.

### Appendix C: Intraband components of $\langle m | \mathcal{V}_i | n \rangle$ in the trivial superconducting state

In this section, we are going to show explicitly that the components of  $\langle m | \mathcal{V}_i | n \rangle$  corresponding to the intraband transitions in the normal phase band structure are zero following Ref. [39]. Using the eigenvectors in Eq. (37) of the BdG Hamiltonian  $H_{\text{BdG}}^{(e)}$ , the components of  $\langle m | \mathcal{V}_i | n \rangle$  which are relevant to the calculation of  $L_{z,2}^{(p)}$  at the zero temperature are given by

$$\langle c, i, \alpha | \partial_t H | v, j, \alpha' \rangle = \sin \frac{\Xi_i - \Xi_j}{2} \langle i, \alpha | \partial_t H_0 | j, \alpha' \rangle. \quad (\text{C1})$$

Note that the right-hand side is zero whenever  $\Xi_i = \Xi_j$ , which is satisfied if  $\xi_i = \xi_j$ . Therefore, no components  $\langle m | \mathcal{V}_i | n \rangle$  corresponding to the intraband transitions in the normal phase band structure are finite. The proof can

be generalized to the case in which the gap function commutes with the normal phase Hamiltonian and preserves the spatio-temporal inversion so that the eigenstates degenerate due to the Kramers' theorem are subject to the gap functions of the same magnitude.

#### Appendix D: Estimation of $L_{z,2}^{(o)}$ when $g_e = g_o$

When  $g_o = g_e$ , we can use  $\langle \sin^2 \chi \rangle_{\text{FS}} = \frac{\ln(\Lambda/T_{c,e})}{\ln(\Lambda/T_{c,o})}$ , and it is possible to find a simple relation between  $L_{z,2}^{(o)}(\Omega)$  and the superconducting transition temperatures  $T_{c,e}$  and  $T_{c,o}$ . Using the expressions for  $T_{c,e}$  and  $T_{c,o}$  in the weak-coupling limit,  $L_{z,2}^{(o)}(\Omega)$  is expressed by

$$\begin{aligned} L_{z,2}^{(o)}(\Omega) &\approx -\frac{1.73N_{\text{tot}}T_{c,e}}{2} \frac{\ln(\Lambda/T_{c,e})}{\ln(\Lambda/T_{c,o})} \ln \frac{T_{c,e}}{T_{c,o}} \\ &\approx -\frac{1.73N_{\text{tot}}T_{c,e}}{2} \ln \frac{T_{c,e}}{T_{c,o}}, \end{aligned} \quad (\text{D1})$$

where  $\Delta_e = 1.73T_{c,e}$  and  $\langle \sin^2 \chi \rangle_{\text{FS}} = \frac{\ln(\Lambda/T_{c,e})}{\ln(\Lambda/T_{c,o})}$  are used to obtain the first line of Eq. (D1) and  $\Lambda \gg T_{c,e}, T_{c,o}$  is used to obtain the second line.

#### Appendix E: Analytical expressions for $\Pi^{(o)}(\Omega)$ in the eSC state and $\Omega_{\text{BS}}$

In this section, an analytical expression for the gap of the BS mode from a subdominant odd parity pairing channel is presented. In general, the gap of this collective mode can be determined by solving  $\det[g_o^{-1} + \Pi^{(o)}(\Omega)] = 0$  within the generalized random-phase approximation formalism, and we are going to calculate each elements of  $\Pi^{(o)}(\Omega)$  for  $|\Omega| < 2\Delta_e$  in appropriate approximations. To get to the point first,

$$\Pi_{11}^{(o)}(\Omega) = \langle \sin^2 \chi \rangle \left\{ \frac{2N_{\text{tot}} \arcsin y}{y/\sqrt{1-y^2}} - \frac{1}{g_e} \right\}, \quad (\text{E1})$$

$$\Pi_{12}^{(o)}(\Omega) \approx \langle \cos^2 \chi \rangle \Pi_{12}^{(e)}(\Omega), \quad (\text{E2})$$

$$\Pi_{22}^{(o)}(\Omega) \approx -\langle \sin^2 \chi \rangle \left\{ \frac{1}{g_e} + N_{\text{tot}} \frac{2y \arcsin y}{\sqrt{1-y^2}} \right\}. \quad (\text{E3})$$

with  $y = \Omega^+ / 2\Delta_e$  and  $N_{\text{tot}} = N_1 + N_2$ , which is used throughout this section. Here,  $N_i$  is the density of states at the Fermi surface from the band  $\xi_i$ . (Counting the Kramer degeneracy,  $2N_{\text{tot}}$  is the total density of states.)

The following formulae are frequently used in the derivation.

$$|\langle \xi_i, s | \sigma_z | \xi_j, s' \rangle| = (1 - \delta_{ss'}) \begin{cases} |\sin \chi| & i = j \\ |\cos \chi| & i \neq j \end{cases}, \quad (\text{E4})$$

$$\langle c, i, s | \tau_y^{(o)} | v, j, s' \rangle = \frac{1}{i} \cos \frac{\Xi_j - \Xi_i}{2} \langle \xi_i, s | \sigma_z | \xi_j, s' \rangle, \quad (\text{E5})$$

$$\langle c, i, s | \tau_x^{(o)} | v, j, s' \rangle = \cos \frac{\Xi_j + \Xi_i}{2} \langle \xi_i, s | \sigma_z | \xi_j, s' \rangle, \quad (\text{E6})$$

$$\frac{1}{g_e} = \sum_i N_i \int_{-\Lambda}^{\Lambda} d\xi_i \frac{1}{E_{c,i}}, \quad (\text{E7})$$

for  $i, j = 1, 2$  and  $s, s' = \alpha, \beta$  derived by using the eigenvectors of  $H_{\text{BdG}}$  in Eq. (37). The last equation is the BCS gap equation with the energy cut-off  $\Lambda$ .

#### 1. $\Pi_{22}^{(o)}(\Omega)$ in the eSC state

For later use, we first evaluate  $\Pi_{22}^{(o)}(0)$  using the identity

$$[\tau_z \sigma_z, G_k^{-1}] = -2i\tau_y^{(o)} \Delta_{e,R} - 4iF_A. \quad (\text{E8})$$

where  $4iF_A \equiv [\sigma_z, H_0]$ . This commutator appears in literature which are concerned with the concept of superconducting fitness [21]. When the Ising-type spin-orbit coupling is ignored ( $\lambda_{\text{Ising}} = 0$ ) in Eq. (1),  $F_A = J_z$  is satisfied. Given the self-consistent gap equation  $2\Delta_{e,R} = -g_e \text{Tr}[\tau_x G_k]$  and  $F_A = J_z$ , we get

$$\Pi_{22}^{(o)}(0) = -\frac{1}{g_e} - \sum_k \frac{\text{Tr}[\tau_y \sigma_z G(k) F_A(\mathbf{k}) G(k)]}{\Delta_{e,R}} \quad (\text{E9})$$

$$= -\frac{1}{g_e} - \frac{2L_{z,2}^{(o)}(0)}{\Delta_{e,R}} \approx -\frac{\langle \sin^2 \chi \rangle}{g_e}, \quad (\text{E10})$$

where we use Eq. (42) for the last approximation.

Now, we calculate  $\Pi_{22}^{(o)}(\Omega)$ . First,  $\Pi_{22}^{(o)}(\Omega)$  at zero-temperature is written as

$$\Pi_{22}^{(o)}(\Omega) = \Pi_{22}^{(o,\text{sig})}(\Omega) + \Pi_{22}^{(o,\text{reg})}(\Omega), \quad (\text{E11})$$

with

$$\Pi_{22}^{(o,\text{sig})}(\Omega) = \sum_{\mathbf{k}} \sum_{i=1,2}^{\checkmark} \frac{4E_{c,i} \sin^2 \chi}{(\Omega^+)^2 - 4E_{c,i}^2}, \quad (\text{E12})$$

$$\Pi_{22}^{(o,\text{reg})}(\Omega) = \sum_{\mathbf{k}} \frac{4 \cos^2 \chi \cos^2 \frac{\Xi_1 - \Xi_2}{2} (E_{c,1} + E_{c,2})}{(\Omega^+)^2 - (E_{c,1} + E_{c,2})^2},$$

The potential singularities of  $\Pi_{22}^{(o,\text{reg})}(\Omega)$  lie at  $\Omega = E_{c,1} + E_{c,2} \gg 2\Delta$ , and thus  $\Pi_{22}^{(o,\text{reg})}(\Omega) \approx \Pi_{22}^{(o,\text{reg})}(0)$  is a good approximation for  $|\Omega| < 2\Delta_e$ . A tedious manipulation easily leads to

$$\Pi_{22}^{(o,\text{reg})}(0) + \sum_{\mathbf{k},i}^{\checkmark} \frac{\cos^2 \chi}{E_{c,i}} = \frac{2L_{z,2}^{(o)}(0)}{-\Delta_e} = \frac{\langle \cos^2 \chi \rangle}{g_e}, \quad (\text{E13})$$

implying  $\Pi_{22}^{(o,\text{reg})}(0) \approx 0$ . In this approximation,  $\Pi_{22}^{(o)}(\Omega) - \Pi_{22}^{(o)}(0)$  turns out to be

$$\Pi_{22}^{(o)}(\Omega) - \Pi_{22}^{(o)}(0) = \sum_{\mathbf{k}} \sum_i^{\checkmark} \frac{(\Omega^+)^2 \sin^2 \chi}{E_{c,i}((\Omega^+)^2 - 4E_{c,i}^2)}$$

$$= -\langle \sin^2 \chi \rangle N_{\text{tot}} \frac{2y \arcsin y}{\sqrt{1-y^2}}. \quad (\text{E14})$$

Therefore, we obtain

$$\Pi_{22}^{(o)}(\Omega) = -\langle \sin^2 \chi \rangle \left( \frac{1}{g_e} + \frac{2N_{\text{tot}} y \arcsin y}{\sqrt{1-y^2}} \right). \quad (\text{E15})$$

Note that this function diverges at  $y = 1$ .

## 2. $\Pi_{12}^{(o)}(\Omega)$ in the eSC state

$\Pi_{12}^{(o)}(\Omega)$  at the zero-temperature is written as

$$\Pi_{12}^{(o)}(\Omega) = \Pi_{12}^{(o,\text{sig})}(\Omega) + \Pi_{12}^{(o,\text{reg})}(\Omega), \quad (\text{E16})$$

with

$$\Pi_{12}^{(o,\text{sig})}(\Omega) = \sum_{\mathbf{k}} \sum_{i=1,2} \frac{2i\Omega^+ \cos \Xi_i \sin^2 \chi}{4E_{c,i}^2 - (\Omega^+)^2}, \quad (\text{E17})$$

$$\Pi_{12}^{(o,\text{reg})}(\Omega) = \sum_{\mathbf{k}} \frac{2i\Omega^+ (\cos \Xi_1 + \cos \Xi_2) \cos^2 \chi}{(E_{c,1} + E_{c,2})^2 - (\Omega^+)^2}.$$

Note that  $\Pi_{12}^{(o,\text{sig})} = \langle \sin^2 \chi \rangle \Pi_{12}^{(e)}$  which is a linear function of  $\Omega$  and only finite when the electronic density of states is asymmetric around  $\xi_i = 0$ . Meanwhile,  $\Pi_{12}^{(o,\text{reg})}(\Omega)$  is negligible in the weak-coupling theory because  $\cos \Xi_1 + \cos \Xi_2 \sim 1$  and  $(E_{c,1} + E_{c,2})^2 - (\Omega^+)^2 \sim 4(\xi_1 - \xi_2)^2 \gg \Lambda\Delta$  with  $\Lambda$  the integration cutoff. Thus, we neglect it, and obtain

$$\Pi_{12}^{(o)}(\Omega) \approx \langle \sin^2 \chi \rangle \Pi_{12}^{(e)}(\Omega). \quad (\text{E18})$$

## 3. $\Pi_{11}^{(o)}(\Omega)$ in the eSC state

$\Pi_{11}^{(o)}(\Omega)$  at the zero-temperature is written as

$$\Pi_{11}^{(o)}(\Omega) = \Pi_{11}^{(o,\text{sig})}(\Omega) + \Pi_{11}^{(o,\text{reg})}(\Omega), \quad (\text{E19})$$

with

$$\Pi_{11}^{(o,\text{sig})}(\Omega) = \sum_{\mathbf{k}} \sum_{i=1,2} \frac{4\xi_i^2 \sin^2 \chi}{E_{c,i} \{(\Omega^+)^2 - 4E_{c,i}^2\}}, \quad (\text{E20})$$

$$\Pi_{11}^{(o,\text{reg})}(\Omega) = \sum_{\mathbf{k}} \frac{2(E_{c,1} + E_{c,2}) \cos^2 \chi}{(\Omega^+)^2 - (E_{c,1} + E_{c,2})^2} Z, \quad (\text{E21})$$

with  $Z = (E_1 E_2 + \xi_1 \xi_2 - \Delta^2)/(2E_1 E_2)$ .  $\Pi_{11}^{(o,\text{reg})}(\Omega)$  is negligible since it is order of  $(\Delta/(\xi_1 - \xi_2))^2$ . Evaluating the singular term  $\Pi_{11}^{(o,\text{sig})}(\Omega)$  at  $\Omega = 0$ , we get

$$\Pi_{11}^{(o)}(0) = -\frac{\langle \sin^2 \chi \rangle}{g_e} + 2\langle \sin^2 \chi \rangle N_{\text{tot}}. \quad (\text{E22})$$

Calculating  $\Pi_{11}^{(o)}(\Omega) - \Pi_{11}^{(o)}(0)$ , we obtain

$$\begin{aligned} \Pi_{11}^{(o)}(\Omega) - \Pi_{11}^{(o)}(0) &= \sum_{\mathbf{k}} \sum_i \frac{\xi_i^2 \sin^2 \chi (\Omega^+)^2}{E_{c,i} \{(\Omega^+)^2 - 4E_{c,i}^2\}} \\ &= 2\langle \sin^2 \chi \rangle N_{\text{tot}} \left( \frac{\arcsin y}{y/\sqrt{1-y^2}} - 1 \right), \end{aligned} \quad (\text{E23})$$

which leads to

$$\Pi_{11}^{(o)}(\Omega) = -\frac{\langle \sin^2 \chi \rangle}{g_e} + \langle \sin^2 \chi \rangle N_{\text{tot}} \frac{2 \arcsin y}{y/\sqrt{1-y^2}}. \quad (\text{E24})$$

Note that  $\Pi_{11}^{(o)}(0) > \Pi_{11}^{(o)}(2\Delta) = \Pi_{22}^{(o)}(0)$  [45, 46], which implies  $\Pi_{11}^{(o)}(\Omega) + \frac{1}{g_o}$  is a regular function for  $|\Omega| < 2\Delta$  because  $\Pi_{11}^{(o)}(\Omega) + \frac{1}{g_o} > 0$  when  $\Pi_{22}^{(o)}(\Omega) + \frac{1}{g_o} = 0$ .

## 4. $\Omega_{\text{BS}}$ in the eSC state

The gap of the BS mode is obtained by finding the zero of  $\det[g_o^{-1} + \Pi^{(o)}(\Omega)] = 0$ . Since  $\Pi_{11}^{(o)}(\Omega)$  is regular and finite for  $|\Omega| < 2\Delta$  and  $\Pi_{12}^{(o)}(\Omega)$  and  $\Pi_{21}^{(o)}$  are expected to be small as we have shown,  $\Omega_{\text{BS}}$  can be accurately approximated by the zero of  $\Pi_{22}^{(o)}(\Omega) + g_o^{-1} = 0$ . Consequently, the semi-analytical expression for  $\Omega_{\text{BS}}$  is given by

$$\frac{2y \arcsin y}{\sqrt{1-y^2}} = \frac{1}{\langle \sin^2 \chi \rangle g_o N_{\text{tot}}} - \frac{1}{g_e N_{\text{tot}}} = \log \frac{T_{c,e}}{T_{c,o}}, \quad (\text{E25})$$

where the last equality is derived under the assumption that the superconducting transition temperatures  $T_{c,e}$  and  $T_{c,o}$  take the BCS-like form  $T_{c,e} \sim \Lambda \exp[-1/g_e N_{\text{tot}}]$  and  $T_{c,o} \sim \Lambda \exp[-1/g_e \langle \sin^2 \chi \rangle N_{\text{tot}}]$ , respectively.

For  $T_{c,o} = 0.87T_{c,e}$ , Eq. (E25) yields  $y = \Omega_{\text{BS}}/2\Delta_e \sim 0.26$  in the eSC state. Therefore, the BS mode in the eSC state is expected to be found below the midst of the superconducting excitation gap.

## 5. The peak intensity from the BS mode in $\tilde{K}_{zz}$

Here, we evaluate the intensity of the Dirac delta peak in  $\tilde{K}_{zz}$  from the BS mode. The peak is mainly attributed to the zero of  $\Pi_{22}^{(o)}(\Omega) + g_o^{-1} = 0$ , and thus we approximate  $[L^{(o)}(g_o^{-1} + \Pi^{(o)})^{-1} R^{(o)}]_{z,z}$  by

$$[L^{(o)}(g_o^{-1} + \Pi^{(o)})^{-1} R^{(o)}]_{z,z} \approx \frac{L_{z,2}^{(o)} R_{2,z}^{(o)}}{\frac{1}{g_o} + \Pi_{22}^{(o)}(\Omega) + i\epsilon}. \quad (\text{E26})$$

As the imaginary part of  $\Pi_{22}^{(o)}(\Omega)$  should be positive for causality, we add an infinitesimal number  $\epsilon$  to  $\Pi_{22}^{(o)}(\Omega)$ . Taking the limit  $\epsilon \rightarrow 0^+$ , we get the Dirac delta peak of the BS mode

$$\frac{L_{z,2}^{(o)} R_{2,z}^{(o)}}{\frac{1}{g_o} + \Pi_{22}^{(o)}(\Omega) + i\epsilon} = |L_{z,2}^{(o)}|^2 \frac{\delta(\Omega - \Omega_{\text{BS}})}{\partial_{\Omega} \Pi_{22}^{(o)}|_{\Omega_{\text{BS}}}} \quad (\text{E27})$$

$$= \frac{\Omega_{\text{BS}} |L_{z,2}^{(o)}|^2}{2(\sin^2 \chi) N_{\text{tot}}} p(\Omega_{\text{BS}}) \delta(\Omega - \Omega_{\text{BS}}),$$

with  $|L_{z,2}^{(o)}|^2 = \frac{\Delta^2 (\cos^2 \chi)^2}{4g_e^2}$  and

$$p(\Omega_{\text{BS}}) = \frac{1 - y_{\text{BS}}^2}{\frac{1}{2N_{\text{tot}}} \left\{ \frac{1}{g_o(\sin^2 \chi)} - \frac{1}{g_e} \right\} + y_{\text{BS}}^2}. \quad (\text{E28})$$

If the solution  $y_{\text{BS}}$  of Eq. (E25) is small, it can be approximated by  $2g_e N_{\text{tot}} y_{\text{BS}}^2 \approx \frac{g_e}{g_o(\sin^2 \chi)} - 1$ . Thus,  $p(\Omega_{\text{BS}})$

is also expected to scale like  $y_{\text{BS}}^{-2}$  for small  $y_{\text{BS}}$  and the intensity is fortified like  $1/\Omega_{\text{BS}}$  for small  $\Omega_{\text{BS}}$ .

This scaling of the peak intensity for small  $\Omega_{\text{BS}}$  is a consequence of the generic properties of the linear response functions rendering  $\det[1/g_o^{-1} + \Pi^{(o)}(\Omega)]$  an even function of  $\Omega$  for  $|\Omega| < 2\Delta_e$ . Therefore, regardless of the control parameter used to lower  $\Omega_{\text{BS}}$ , the peak intensity, or height, will increase as  $\Omega_{\text{BS}}$  is lowered.

- 
- [1] R. Joynt and L. Taillefer, The superconducting phases of  $\text{UPt}_3$ , *Rev. Mod. Phys.* **74**, 235 (2002).
- [2] K. Ishida, D. Ozaki, T. Kamatsuka, H. Tou, M. Kyogaku, Y. Kitaoka, N. Tateiwa, N. K. Sato, N. Aso, C. Geibel, and F. Steglich, Spin-Triplet Superconductivity in  $\text{UNi}_2\text{Al}_3$  Revealed by the  $^{27}\text{Al}$  Knight Shift Measurement, *Phys. Rev. Lett.* **89**, 037002 (2002).
- [3] A. P. Mackenzie, T. Scaffidi, C. W. Hicks, and Y. Maeno, Even odder after twenty-three years: the superconducting order parameter puzzle of  $\text{Sr}_2\text{RuO}_4$ , *npj Quantum Materials* **2**, 40 (2017).
- [4] A. Pustogow, Y. Luo, A. Chronister, Y. S. Su, D. A. Sokolov, F. Jerzembeck, A. P. Mackenzie, C. W. Hicks, N. Kikugawa, S. Raghu, E. D. Bauer, and S. E. Brown, Constraints on the superconducting order parameter in  $\text{Sr}_2\text{RuO}_4$  from oxygen-17 nuclear magnetic resonance, *Nature* **574**, 72 (2019).
- [5] K. Ishida, M. Manago, K. Kinjo, and Y. Maeno, Reduction of the  $^{17}\text{O}$  Knight shift in the superconducting state and the heat-up effect by NMR pulses on  $\text{Sr}_2\text{RuO}_4$ , *J. Phys. Soc. Japan* **89**, 1 (2020).
- [6] A. N. Petsch, M. Zhu, M. Enderle, Z. Q. Mao, Y. Maeno, I. I. Mazin, and S. M. Hayden, Reduction of the Spin Susceptibility in the Superconducting State of  $\text{Sr}_2\text{RuO}_4$  Observed by Polarized Neutron Scattering, *Phys. Rev. Lett.* **125**, 217004 (2020).
- [7] H. G. Suh, H. Menke, P. M. R. Brydon, C. Timm, A. Ramirez, and D. F. Agterberg, Stabilizing even-parity chiral superconductivity in  $\text{Sr}_2\text{RuO}_4$ , *Phys. Rev. Res.* **2**, 032023 (2020).
- [8] S. Käser, H. U. R. Strand, N. Wentzell, A. Georges, O. Parcollet, and P. Hansmann, Interorbital singlet pairing in  $\text{Sr}_2\text{RuO}_4$ : A Hund's superconductor, *Phys. Rev. B* **105**, 155101 (2022).
- [9] V. Kozii and L. Fu, Odd-Parity Superconductivity in the Vicinity of Inversion Symmetry Breaking in Spin-Orbit-Coupled Systems, *Phys. Rev. Lett.* **115**, 207002 (2015).
- [10] T. Schumann, L. Galletti, H. Jeong, K. Ahadi, W. M. Strickland, S. Salmani-Rezaie, and S. Stemmer, Possible signatures of mixed-parity superconductivity in doped polar  $\text{SrTiO}_3$  films, *Phys. Rev. B* **101**, 100503 (2020).
- [11] Y. Wang, G. Y. Cho, T. L. Hughes, and E. Fradkin, Topological superconducting phases from inversion symmetry breaking order in spin-orbit-coupled systems, *Phys. Rev. B* **93**, 1 (2016).
- [12] Y. Wang and L. Fu, Topological Phase Transitions in Multicomponent Superconductors, *Phys. Rev. Lett.* **119**, 187003 (2017).
- [13] S. Khim, J. F. Landaeta, J. Banda, N. Bannor, M. Brando, P. M. R. Brydon, D. Hafner, R. Küchler, R. Cardoso-Gil, U. Stockert, A. P. Mackenzie, D. F. Agterberg, C. Geibel, and E. Hassinger, Field-induced transition within the superconducting state of  $\text{CeRh}_2\text{As}_2$ , *Science* **373**, 1012 (2021).
- [14] D. Hafner, P. Khanenko, E.-O. Eljaouhari, R. Küchler, J. Banda, N. Bannor, T. Lühmann, J. F. Landaeta, S. Mishra, I. Sheikin, E. Hassinger, S. Khim, C. Geibel, G. Zwicknagl, and M. Brando, Possible Quadrupole Density Wave in the Superconducting Kondo Lattice  $\text{CeRh}_2\text{As}_2$ , *Phys. Rev. X* **12**, 011023 (2022).
- [15] D. Maruyama, M. Sigrist, and Y. Yanase, Locally non-centrosymmetric superconductivity in multilayer systems, *J. Phys. Soc. Japan* **81**, 1 (2012).
- [16] M. Sigrist, D. F. Agterberg, M. H. Fischer, J. Goryo, F. Loder, S. H. Rhim, D. Maruyama, Y. Yanase, T. Yoshida, and S. J. Youn, Superconductors with staggered non-centrosymmetry, *J. Phys. Soc. Japan* **83**, 1 (2014).
- [17] A. M. Clogston, Upper limit for the critical field in hard superconductors, *Phys. Rev. Lett.* **9**, 266 (1962).
- [18] G. Sarma, On the influence of a uniform exchange field acting on the spins of the conduction electrons in a superconductor, *J. Phys. Chem. Solids* **24**, 1029 (1963).
- [19] Y. Maeno, S. Kittaka, T. Nomura, S. Yonezawa, and K. Ishida, Evaluation of spin-triplet superconductivity in  $\text{Sr}_2\text{RuO}_4$ , *J. Phys. Soc. Japan* **81**, 1 (2012).
- [20] D. C. Cavanagh, T. Shishidou, M. Weinert, P. M. R. Brydon, and D. F. Agterberg, Nonsymmorphic symmetry and field-driven odd-parity pairing in  $\text{CeRh}_2\text{As}_2$ , *Phys. Rev. B* **105**, L020505 (2022).
- [21] D. Möckli and A. Ramirez, Two scenarios for superconductivity in  $\text{CeRh}_2\text{As}_2$ , *Phys. Rev. Res.* **3**, 023204 (2021).
- [22] T. Yoshida, M. Sigrist, and Y. Yanase, Pair-density wave states through spin-orbit coupling in multilayer superconductors, *Phys. Rev. B* **86**, 1 (2012).
- [23] K. Machida, Violation of the Pauli-Clogston limit in a heavy Fermion superconductor  $\text{CeRh}_2\text{As}_2$ -Duality of itinerant and localized 4f electrons, *Phys. Rev. B* **184509**, 1 (2022).
- [24] J. A. Sauls, On the Excitations of a Balian-Werthamer Superconductor, *J Low Temp Phys* **208**, 87 (2022).
- [25] A. Bardasis and J. R. Schrieffer, Excitons and Plasmons in Superconductors, *Phys. Rev.* **121**, 1050 (1961).
- [26] T. Böhm, A. F. Kemper, B. Moritz, F. Kretzschmar,



- B. Muschler, H. M. Eiter, R. Hackl, T. P. Devereaux, D. J. Scalapino, and H. H. Wen, Balancing act: Evidence for a strong subdominant d-wave pairing channel in  $\text{Ba}_{0.6}\text{K}_{0.4}\text{Fe}_2\text{As}_2$ , *Phys. Rev. X* **4**, 1 (2014).
- [27] G. He, D. Li, D. Jost, A. Baum, P. P. Shen, X. L. Dong, Z. X. Zhao, and R. Hackl, Raman Study of Cooper Pairing Instabilities in  $\text{Li}_{1-x}\text{Fe}_x\text{OHFeSe}$ , *Phys. Rev. Lett.* **125**, 1 (2020).
- [28] P. W. Anderson, Random-phase approximation in the theory of superconductivity, *Phys. Rev.* **112**, 1900 (1958).
- [29] G. Rickayzen, Collective excitations in the theory of superconductivity, *Phys. Rev.* **115**, 795 (1959).
- [30] D. Möckli, Y. Yanase, and M. Sigrist, Orbitaly limited pair-density-wave phase of multilayer superconductors, *Phys. Rev. B* **97**, 144508 (2018).
- [31] R. Balian and N. R. Werthamer, Superconductivity with pairs in a relative  $p$  wave, *Phys. Rev.* **131**, 1553 (1963).
- [32] Y. Nambu, Quasi-Particles and Gauge Invariance in the Theory of Superconductivity, *Phys. Rev.* **117**, 648 (1960).
- [33] A. Skurativska, M. Sigrist, and M. H. Fischer, Spin response and topology of a staggered-Rashba superconductor, *Phys. Rev. Res.* **3**, 033133 (2021).
- [34] J. F. Landaeta, P. Khanenko, D. C. Cavanagh, C. Geibel, S. Khim, S. Mishra, I. Sheikin, P. M. R. Brydon, D. F. Agterberg, M. Brando, and E. Hassinger, Field-Angle Dependence Reveals Odd-Parity Superconductivity in  $\text{CeRh}_2\text{As}_2$ , *Phys. Rev. X* **12**, 031001 (2022).
- [35] L. D. Landau and E. M. Lifshitz, *Statistical Physics: Volume 5*, Vol. 5 (Elsevier, 2013).
- [36] R. Boyack and P. L. Lopes, Electromagnetic response of superconductors in the presence of multiple collective modes, *Phys. Rev. B* **101**, 94509 (2020).
- [37] S. Maiti and P. J. Hirschfeld, Collective modes in superconductors with competing s- and d-wave interactions, *Phys. Rev. B* **92**, 094506 (2015).
- [38] G. Giuliani and G. Vignale, *Quantum Theory of the Electron Liquid* (Cambridge University Press, 2005).
- [39] J. Ahn and N. Nagaosa, Theory of optical responses in clean multi-band superconductors, *Nat. Commun.* **12**, 1617 (2021).
- [40] T. Kamatani, S. Kitamura, N. Tsuji, R. Shimano, and T. Morimoto, Optical response of the Leggett mode in multiband superconductors in the linear response regime, *Phys. Rev. B* **105**, 094520 (2022).
- [41] J. W. F. Venderbos, V. Kozii, and L. Fu, Odd-parity superconductors with two-component order parameters: Nematic and chiral, full gap, and Majorana node, *Phys. Rev. B* **94**, 180504 (2016).
- [42] M. Kibune, S. Kitagawa, K. Kinjo, S. Ogata, M. Manago, T. Taniguchi, K. Ishida, M. Brando, E. Hassinger, H. Rosner, C. Geibel, and S. Khim, Observation of Antiferromagnetic Order as Odd-Parity Multipoles inside the Superconducting Phase in  $\text{CeRh}_2\text{As}_2$ , *Phys. Rev. Lett.* **128**, 057002 (2022).
- [43] N. A. Hackner and P. M. R. Brydon, (unpublished).
- [44] S. Tewari, T. D. Stanescu, J. D. Sau, and S. Das Sarma, Topologically non-trivial superconductivity in spin-orbit-coupled systems: bulk phases and quantum phase transitions, *New J. Phys.* **13**, 065004 (2011).
- [45] J. A. Sauls and T. Mizushima, On the Nambu fermion-boson relations for superfluid  $^3\text{He}$ , *Phys. Rev. B* **95**, 094515 (2017).
- [46] Y. Nambu, Fermion-Boson relations in BCS-type theories, *Physica D: Nonlinear Phenomena* **15**, 147 (1985).